Biogeosciences Discuss., 11, 17861–17923, 2014
www.biogeosciences-discuss.net/11/17861/2014/
doi:10.5194/bgd-11-17861-2014

Biogeosciences Discussions
Open Access

Iron budgets for three distinct biogeochemical sites around the Kerguelen archipelago (Southern Ocean) during the natural fertilisation experiment KEOPS-2

A. R. Bowie[1,2,3], P. van der Merwe[1], F. Quéroué[1,2,3], T. Trull[1,4], M. Fourquez[2,5], F. Planchon[3], G. Sarthou[3], F. Chever[3,*], A. T. Townsend[6], I. Obernosterer[5], J.-B. Sallée[7,8,9], and S. Blain[5]

[1]Antarctic Climate and Ecosystems Cooperative Research Centre (ACE CRC), Private Bag 80, Hobart, Tasmania, Australia
[2]Institute for Marine and Antarctic Studies (IMAS), University of Tasmania, Private Bag 129, Hobart, Tasmania, Australia
[3]Laboratoire des Sciences de l'Environnement Marin (LEMAR), UMR6539 UBO/CNRS/IRD/IFREMER, Institut Universitaire Européen de la Mer (IUEM), Technopole Brest Iroise, 29280 Plouzané, France
[4]CSIRO Marine and Atmospheric Research, Castray Esplanade, Hobart, Tasmania, Australia

[5]Université Pierre et Marie, Laboratoire d'Océanographie Microbienne (LOMIC), UMR 7621 CNRS UPMC, Avenue du Fontaulé 66650 Banyuls sur mer, France
[6]Central Science Laboratory (CSL), University of Tasmania, Private Bag 74, Hobart, TAS 7001, Australia
[7]Sorbonne Universités, UPMC Univ., Paris 06, UMR 7159, LOCEAN-IPSL, F-75005, Paris, France
[8]CNRS, UMR 7159, LOCEAN-IPSL, F-75005, Paris, France
[9]British Antarctic Survey, High Cross, Cambridge, CB3 0ET, UK
[*]now at: National Oceanography Centre, University of Southampton Waterfront Campus, European Way, Southampton SO14 3ZH, UK

Received: 19 November 2014 – Accepted: 24 November 2014 – Published: 19 December 2014

Correspondence to: A. R. Bowie (andrew.bowie@utas.edu.au)

Published by Copernicus Publications on behalf of the European Geosciences Union.

BGD
11, 17861–17923, 2014

Abstract

Iron availability in the Southern Ocean controls phytoplankton growth, community composition and the uptake of atmospheric CO_2 by the biological pump. The KEOPS-2 experiment took place around the Kerguelen plateau in the Indian sector of the Southern Ocean, a region naturally fertilised with iron at the scale of hundreds to thousands of square kilometres, producing a mosaic of spring blooms which showed distinct biological and biogeochemical responses to fertilisation. This paper presents biogeochemical iron budgets (incorporating vertical and lateral supply, internal cycling, and sinks) for three contrasting sites: an upstream high-nutrient low-chlorophyll reference, over the plateau, and in the offshore plume east of Kerguelen Island. These budgets show that distinct regional environments driven by complex circulation and transport pathways are responsible for differences in the mode and strength of iron supply, with vertical supply dominant on the plateau and lateral supply dominant in the plume. Iron supply from "new" sources to surface waters of the plume was double that above the plateau and 20 times greater than at the reference site, whilst iron demand (measured by cellular uptake) in the plume was similar to the plateau but 40 times greater than the reference. "Recycled" iron supply by bacterial regeneration and zooplankton grazing was a relative minor component at all sites (< 8 % of "new" supply), in contrast to earlier findings from other biogeochemical iron budgets in the Southern Ocean. Over the plateau, a particulate iron dissolution term of 2.5 % was invoked to balance the budget; this approximately doubled the standing stock of dissolved iron in the mixed layer. The exchange of iron between dissolved, biogenic and lithogenic particulate pools was highly dynamic in time and space, resulting in a decoupling of iron supply and carbon export and, importantly, controlling the efficiency of fertilisation.

BGD
11, 17861–17923, 2014

1 Introduction

The concentration of carbon dioxide in earth's atmosphere and therefore earth's climate is highly sensitive to modification of the carbon (C) cycle due to the growth of phytoplankton in the Southern Ocean (Sarmiento and Gruber, 2006). These single-cell plants remove inorganic carbon from surface seawater during photosynthesis, which can be directly transferred into the deep sea when they die and sink, or indirectly through the food web. The Southern Ocean is responsible for 30 % of global ocean carbon export (Schlitzer, 2002). As first demonstrated over 20 years ago, phytoplankton growth in the Southern Ocean is limited by the availability of the micro-nutrient trace element iron (Fe; Martin, 1990). Low dissolved iron (dFe) availability limits the annual uptake of atmospheric carbon dioxide (CO_2) by the Southern Ocean (Boyd et al., 2000), shapes phytoplankton species composition and physiology (Assmy et al., 2013), the cycling of other nutrient elements (Moore and Doney, 2007) and thus the structure of the entire marine ecosystem (Boyd and Ellwood, 2010).

Artificial mesoscale ocean iron fertilisation experiments have unequivocally demonstrated the role of Fe in setting phytoplankton productivity, biomass and community structure in high nutrient low chlorophyll (HNLC) regions (Boyd et al., 2007). However, the "carbon sequestration efficiency" of ocean fertilisation as a means to sequester atmospheric CO_2 (calculated as the additional (net) C that is exported from surface waters into the deep (> 1000 m) ocean for a given addition of Fe) varies widely between experiments and is considerably less than estimates from the early iron fertilisation experiments (see discussion in de Baar et al., 2008). This is likely due to the rapid grazing of phytoplankton in surface waters (Boyd et al., 2007) and the loss of the added Fe by its precipitation and scavenging onto sinking particles (Bowie et al., 2001).

The natural resupply of iron to Fe-depleted waters is a more efficient process (Blain et al., 2007), although in part this depends on the mode of Fe delivery (e.g., from above or below), the ability of organic ligands to keep the supplied Fe in solution (Gerringa et al., 2008), and for continued ocean fertilisation is in part reliant on the

BGD
11, 17861–17923, 2014

concurrent supply of other major nutrients. In the Indian sector of the subantarctic Southern Ocean, natural Fe supply from the Kerguelen plateau (Blain et al., 2007) and Crozet Islands (Pollard et al., 2009) results in increased phytoplankton biomass during summer, with chlorophyll levels increasing to more than an order of magnitude above background (de Baar et al., 2005); as revealed by NASA MODIS satellite chlorophyll climatology for January (2003–2010) (Westberry et al., 2013). Previous studies of the blooms in these localised "natural laboratory" experiments have provided invaluable insights into mechanisms linking iron fertilisation and carbon cycling in the Southern Ocean, especially since they can address the effects of persistent, varying and multiple Fe sources that are not accessible through deliberate artificial mesoscale fertilisation experiments.

The KEOPS-1 (KErguelen: compared study of Ocean and Plateau in Surface waters) experiment which took place in the late austral summer of January–February 2005 demonstrated that this natural fertilisation of the Southern Ocean resulted in dramatic changes in the functioning of the ecosystem with large impacts on the biogeochemical cycles (Blain et al., 2007, 2008a). These observations of the bloom were largely confined to the plateau region, where vertical upwelled supply from the plateau sediments (Blain et al., 2008b; Zhou et al., 2014) and lateral advection of water that had been in contact with the continental shelf of Heard Island to the south (Chever et al., 2010), were the dominant sources of dissolved and particulate Fe. The interaction of waters, islands and plateau of the Kerguelen archipelago with several circumpolar fronts of the Southern Ocean allowed us to make a first attempt at placing our regional KEOPS-1 observations within a broader basin scale context (Blain et al., 2007).

The KEOPS-2 project was designed to improve the spatial and temporal coverage of the Kerguelen region. During KEOPS-2, which was approved as a GEOTRACES Process Study[1], we studied the region above and downstream of the plateau and observed a massive natural iron fertilisation at the scale of hundreds of thousands of

[1] http://www.geotraces.org/cruises/cruise-summary/68-science/process-studies/206-geotraces-process-studies

BGD
11, 17861–17923, 2014

square kilometres. This produced a patchwork of blooms with diverse biological and biogeochemical responses, as detailed in the multiple studies in this special issue of Biogeosciences. KEOPS-2 was also carried out in the austral spring to document the early stages of the bloom and to complement results of KEOPS-1 obtained in late summer during the start of the decline of the bloom, with a principal aim to better constrain the mechanism of Fe supply to surface waters earlier in the season.

Since Fe is actively taken up into phytoplankton, and transferred throughout the food-web, including removal by particle settling and remineralisation in deep waters, the assessment of its availability is quite complex and cannot be judged from dFe levels in surface waters alone (Breitbarth et al., 2010). Advances in chemical oceanographic techniques for trace elements through the GEOTRACES program (SCOR Working Group, 2007) now allow the measurement of Fe associated with different phases (dissolved and particulate), internal biological recycling and Fe export from surface waters. The results from earlier iron biogeochemical budgets for FeCycle (Boyd et al., 2005; Frew et al., 2006), KEOPS-1 (Blain et al., 2007; Chever et al., 2010), CROZEX (Planquette et al., 2007, 2009) and SAZ-Sense (Bowie et al., 2009) have highlighted that the dominant "new" Fe fluxes are associated with the particulate phase. Particles thus represent an important transport vector for trace metals in the marine ecosystem, although their bioavailability or transfer into a bioavailable fraction remains uncertain. Suspended particles have also been shown to be important aspects of sedimentary, boundary layer Fe sources and export processes (Tagliabue et al., 2009; Homoky et al., 2013; Marsay et al., 2014; Wadley et al., 2014), with particles being transported laterally over hundreds of kilometres (Lam et al., 2006; Lam and Bishop, 2008; Cullen et al., 2009). The biological cycling of particulate Fe may therefore be the most important aspect of the complete Fe biogeochemical cycle especially since earlier budgets have demonstrated that biological Fe "demand" cannot be satisfied by the "new" Fe supply (Boyd et al., 2005; Blain et al., 2007; Sarthou et al., 2008; Bowie et al., 2009; de Jong et al., 2012). A simple one dimensional vertical model that correctly represented the input of dFe to surface waters during KEOPS-1 did not accurately represent the supply of other geo-

BGD
11, 17861–17923, 2014

chemical tracers or particulate Fe (Blain et al., 2007), and the role of dissolved and particulate Fe earlier in the season (winter stock) in the Kerguelen region has yet to be quantified.

This paper presents a short-term (days–weeks) Fe budget for the period of the KEOPS-2 study for each of three process sites: (i) a "Plateau" bloom site (A3) on the central Kerguelen plateau studied during late summer on KEOPS-1 and reoccupied during spring on KEOPS-2, (ii) a "Plume" bloom site (E) east of Kerguelen Island which was located within a quasi-stationary, bathymetrically trapped recirculation feature near the Polar Front, (iii) a "Reference" site (R-2) south of the Polar Front (PF) and upstream (southwest) of Kerguelen in HNLC waters. We focus on mixed layer integrated pools of dissolved Fe and particulate Fe (which we further separate into biogenic and lithogenic fractions using elemental normalisers), estimate the fluxes of Fe associated with "new" and "recycled" Fe sources, and compare Fe supply and demand with implications for bloom duration and magnitude. Our observations also include particulate measurements in both suspended water column (ISP) and sinking export (P-trap) particles below the mixed layer, with linkage to food web processes via discussion of iron-to-carbon (Fe/C) ratios. Finally, we present a seasonal comparison of our springtime budget for KEOPS-2 with late summer observations from KEOPS-1, and also make comparison with findings from other sectors of the Southern Ocean subjected to natural Fe fertilisation (e.g., Frew et al., 2006 and Boyd et al., 2005 for "FeCycle1" southeast of New Zealand; Ellwood et al., 2014 for "FeCycle2" east of New Zealand; Bowie et al., 2009 for "SAZ-Sense" south of Tasmania; Planquette et al., 2011 for "CROZEX" near the Crozet Islands; and Zhou et al., 2010 for "Blue Water Zone" near the western Antarctic Peninsula). The observations of dFe (Quéroué et al., 2014) and particulate trace metals (van der Merwe et al., 2014) are detailed in companion papers in this special issue, to allow the current paper to focus explicitly on construction of iron budgets; however the three papers should be seen as a collective whole.

BGD
11, 17861–17923, 2014

2 Material and methods

2.1 Study area

The KEOPS-2 (KErguelen: compared study of Ocean and Plateau in Surface waters) expedition was carried out in the Indian sector of the Southern Ocean in the vicinity of the Kerguelen plateau between 7 October and 30 November 2011 on the M.D. *Marion Dufresne* (Fig. 1a). The plateau of the Kerguelen archipelago is a northwest-southeast seafloor feature approximately 500 m deep and is constrained by the Kerguelen Islands to the north and the smaller volcanic Heard/McDonald Islands to the south. Our study was conducted in early austral spring when phytoplankton biomass was developing rapidly and forming a mosaic of phytoplankton blooms in the region (Trull et al., 2014; Blain et al., 2014a; Lasbleiz et al., 2014). Since sampling at the different stations took place at different times over the ∼ 7 week study, our observations also provide a temporal sequence relative to the development of surface biomass.

The Kerguelen bloom has two main features, a northern branch that extends northeast of the island into waters both south and north of the PF, and a larger bloom covering ∼ 45 000 km^2 south of the PF and largely constrained to the shallow bathymetry of the Kerguelen plateau (< 700 m) (Mongin et al., 2008; Supplement in Trull et al., 2014) (Figs. 1b and 2). Thirty-two stations were sampled during KEOPS-2, often with repeat visits. Here we focus on three study sites, namely: plateau A3, plume E and reference R-2 (Fig. 1). Two visits were made to A3 at the start (A3-1) and end (A3-2) of the voyage (28 days apart), and five visits were made to site E (over 21 days) to document the bloom development. Based on the trajectories of surface drifters, stations E-1, E-3 and E-5 were taken tracking the middle of a recirculation region (d'Ovidio et al., 2014), so that they can be considered as pseudo-Lagrangian and their succession in time can be considered a first order time series. Full details of other stations and sampling designed to document the meridional and zonal extensions of the blooms on the plateau and to the east of Kerguelen are contained in Blain et al. (2014a).

BGD
11, 17861–17923, 2014

The hydrology and circulation around and above the Kerguelen plateau have been described by Park et al. (2008a, b, 2014a), van Beek et al. (2008), Zhang et al. (2008) and Zhou et al. (2014). The mean circulation is shown in Fig. 1b. Briefly, the Kerguelen plateau constitutes a barrier to the eastward flowing Antarctic Circumpolar Current (ACC), the main jets of which are the Sub-Antarctic Front (SAF) and PF. Most of the ACC is deflected north of the Kerguelen Islands as Sub-Antarctic Surface Water (SASW) but some filaments passes between the Kerguelen Islands and Heard Island (as the PF) and further south between Heard Island and Antarctica (Roquet et al., 2009). Above the plateau, the remainder of the ACC comes from the western part of the plateau. Currents of AASW travelling along the western flank of the plateau are deflected south and east of Heard Island as a branch of the Fawn Trough Current (FTC) (Sokolov and Rintoul, 2009), before travelling in a broadly northwest direction up along the eastern shelf-break. The water flow is then deflected toward the east of Kerguelen Island, where there is an intense mixing zone consisting of mesoscale eddies which travel many thousands of kilometres in the ACC towards the Australian sector of the Southern Ocean.

2.2 Sampling

All trace metal sampling and analytical procedures followed recommended protocols in the cookbook[2] published by the international program GEOTRACES as closely as possible (Bishop et al., 2012; Cutter and Bruland, 2012; Planquette and Sherrell, 2012). All methods have been successfully used previously by this team during the KEOPS-1 (Blain et al., 2008b) and SAZ-Sense projects (Bowie et al., 2009).

2.2.1 Trace metal rosette (TMR)

Water column samples were collected using 10 L externally-closing, Teflon-lined Niskin-1010X bottles deployed on an autonomous 1018 intelligent rosette system (spe-

[2]http://www.geotraces.org/libraries/documents/Intercalibration/Cookbook.pdf

BGD
11, 17861–17923, 2014

cially adapted for trace metal work, General Oceanics Inc.). The polyurethane-powder-coated aluminium rosette frame was suspended on Kevlar rope which passed through a clean block with a plastic sheave (General Oceanics) and was lowered to a maximum depth of 1300 m. Bottles were tripped at pre-programmed depths using a pressure sensor as the trace metal rosette was being raised through the water column at approximately 0.5 m s^{-1}.

All sample processing was carried out under an ISO class 5 trace-metal-clean laminar flow bench in a HEPA filtered-air clean container, with all materials used for sample handling thoroughly acid-washed. Samples were drawn through C-Flex tubing (Cole Parmer) and filtered in-line through 0.2 µm pore-size acid-washed capsules (Pall Supor membrane Acropak 200 or Sartorius Sartobran 300 filters). The dissolved fraction is thus likely to contain colloids and small particles < 0.2 µm in diameter (Bowie and Lohan, 2009). All transfer tubes, filtering devices and sample containers were rinsed liberally with sample before final collection in 125 mL Nalgene LDPE bottles. Seawater samples were acidified within 24 h of collection using 2 mL of concentrated ultrapure hydrochloric acid (HCl, Seastar BASELINE grade) per L of sample, resulting in an approximate final pH of 1.8, double bagged and stored for at least 24 h at ambient temperature until analysis.

2.2.2 In situ pumps (ISPs)

Suspended particles for trace elemental analysis were collected using 11 large-volume in situ pumps (McLane Research Laboratories WTS6-1-142LV and Challenger Oceanics pumps), suspended simultaneously at pre-chosen depths, following methods reported in Bowie et al. (2009). Up to 2000 L of seawater was filtered across a 142 mm diameter stack (134 mm diameter active area) consisting of a 53 µm nylon pre-filter screen (NYTEX) followed by a QMA quartz fibre filter (1 µm nominal pore size; Sartorius). The QMA filter was supported by a 350 µm polyester mesh which was placed on top of the Teflon PFA grid of the pump housing. Prior to use, NYTEX screens were conditioned by soaking in 5 % H_2SO_4, rinsed 3× with Milli-Q grade water, dried at ambient

BGD
11, 17861–17923, 2014

temperature under a laminar flow hood and stored in clean plastic Ziploc® bags. QMA filters were conditioned for trace-metal analysis (pre-combustion and acid cleaning) following Bowie et al. (2010). Upon recovery of the pumps, sub-samples were taken from the QMA filters using a circular plastic punch (14 mm diameter) and by cutting the nylon mesh using ceramic scissors. Filters were dried under a laminar flow bench and stored at −18 °C in acid-washed PCR trays until further analysis in the home laboratory. The 1–53 µm and > 53 µm size fractions were digested and analysed separately, and the particulate iron (pFe) reported here is the sum of both fractions. The ISP pumps were shown to be efficient in capturing large (> 53 µm) particles (Planchon et al., 2014).

2.2.3 Free-floating traps (P-trap)

Sinking particles for trace elemental analysis were collected using PPS3/3 free-floating sediment traps (Technicap, France), specially adapted for trace metals, deployed at 200 m. Traps were deployed for 5.3, 5.1, 1.9 and 1.5 days at stations E-1, E-3, A3-2 and E-5, respectively. The trap deployed at station R-2 was lost and not recovered. Traps drifted between 10 and 43 km over the course of the deployment. Full details of the trap deployments are given in Laurenceau et al. (2014) and Planchon et al. (2014). Samples for trace elemental analysis were collected in three separate acid-washed cups (dedicated for trace metals) containing a low trace metal brine solution (salinity ~ 60), each opened for either 1, 3, 8 or 12 h (depending on the station). Upon recovery, cups were taken to a clean room and particles filtered off-line onto a 47 mm diameter, 2 µm porosity polycarbonate filter under gentle vacuum using a Teflon PFA unit (Savillex Corp., USA), equipped with a 350 µm pre-screen (to exclude zooplankton).

BGD
11, 17861–17923, 2014

2.3 Analysis

2.3.1 Dissolved iron

Dissolved Fe (dFe) was determined shipboard by flow injection analysis with chemiluminescence detection (FI-CL) using in-line preconcentration on an 8-hydroxyquinoline chelating resin (adapted from Obata et al., 1993; de Jong et al., 1998 and Sarthou et al., 2003). Dissolved Fe data were quality controlled against the SAFe ("Sampling and Analysis of Fe") standard reference materials (Johnson et al., 2007). Full data including certification results and analytical figures of merit are reported in Quéroué et al. (2014).

2.3.2 Particulate iron

Sampled particles were acid extracted in 1 mL concentrated HNO_3 (Seastar Baseline) for 12 h on a DigiPREP HP Teflon hotplate supplied with HEPA filtered air (SCP Science) at 120 °C using 15 mL Teflon PFA Savillex vials. Digest solutions were diluted with 10 mL ultra-high purity water to 10 % HNO_3 and spiked with 10 ppb indium as internal standard prior to analysis by sector field inductively coupled plasma mass spectrometry (Finnigan ELEMENT 2, Thermo Scientific), following Bowie et al. (2010). Recoveries from the analysis of the Community Bureau of Reference plankton certified reference material BCR-414 were excellent, with a 101 % recovery ($n = 3$) for pFe. Full data are reported in van der Merwe et al. (2014).

2.3.3 Particulate organic carbon and nitrogen

For particulate organic carbon (POC) and particulate nitrogen (PN) analyses, QMA quartz filters from the ISPs were sub-sampled in a flow-bench using a 14 mm diameter plastic punch, transferred to silver foil cups (Sercon brand p/n SC0037). Samples were also collected from the P-traps for POC and PN analyses (see Laurenceau et al., 2014). Samples were treated with a 40 µL aliquot of 2 N HCl to remove carbonates

BGD
11, 17861–17923, 2014

(King et al., 1998), dried at 60 °C for 48 h, and stored in a desiccator until analysis using a Thermo-Finnigan Flash EA1112 elemental analyzer (using sulfanilamide standards) at the Central Science Laboratory, University of Tasmania. The > 53 µm fraction was treated in the same way at the Vrije Universiteit Brussel, after first transferring the material from one fourth of the screen using pre-filtered seawater onto 25 mm diameter, 1.0 µm pore size silver membrane filters (Sterlitech, Concord). Blank corrections for the pump samples were estimated from filters prepared identically but not deployed on the ISPs, and for the trap samples by re-filtering the pre-filtered seawater. All blank corrections were less than 2 % for all samples. The sub-sampling introduces uncertainties of 5–10 % from inhomogeneous filter coverage that exceeds the analytical uncertainty of the POC analysis of ∼ 1 % (Trull et al., 2014).

2.4 Biological iron cycling

2.4.1 Iron uptake

Trace metal clean seawater was collected from the mixed layer (20–40 m) using the TMR, transferred into acid-washed polycarbonate bottles and 0.2 nmol L^{-1} (final concentration) of enriched ^{55}Fe as $FeCl_3$ added (1.83×10^3 Ci mol^{-1} of specific activity, Perkin Elmer). Bottles were placed at in situ temperature in on-deck incubators continuously fed by surface seawater. Incubations were conducted for 24 h (sunrise to sunrise) at several light intensity levels (75, 45, 25, 16, 4, and 1 % of photosynthetically-active radiation; PAR). For stations R-2, A3-1, E-1 and E-3, seawater was prefiltered on a 25 µm mesh size before ^{55}Fe was added. After incubation, 300 mL of seawater was passed through 0.2 µm pore-size nitrocellulose filters (47 mm diameter, Nuclepore). To determine intracellular Fe uptake rates, ^{55}Fe not incorporated by cells was removed immediately after filtration using 6 mL of a Ti-citrate-EDTA washing solution for 2 min, followed by rinsing 3 times with 5 mL of 0.2 µm filtered-seawater for 1 min (Hudson and Morel, 1989; Tang and Morel, 2006). The filters were placed into plastic vials and 10 mL of the scintillation cocktail "Filtercount" (Perkin Elmer) added. Vials were agitated for 24 h be-

BGD
11, 17861–17923, 2014

fore the radioactivity on filters was counted with the Tricarb® scintillation counter (precision < 10 %). Controls were obtained with 300 mL of microwave-sterilized seawater (750 W for 5 min) incubated and treated the same way. Sub-samples for enumeration by flow cytometry were collected from each bottle just before the filtration step. Cells were fixed in glutaraldehyde (1 %) and kept frozen (−80 °C) until processing and analysis. Data were corrected by blank subtraction and Fe uptake rates normalised to the concentration of Fe in each incubation (in situ dFe and ^{55}Fe added). Further details are given in Fourquez et al. (2014).

2.4.2 Iron remineralisation

Since iron regeneration was not measured directly by experiment during KEOPS-2, we used the following approach to calculate iron regeneration fluxes. Bacterial Fe regeneration was estimated from bacterial turnover times determined from bacterial production and biomass (Christaki et al., 2014), assuming all loss of bacterial biomass through viral lysis and flagellate grazing resulted in the regeneration of Fe (Strzepek et al., 2005), and using a bacterial iron quota of 7.5 µmol Fe (mol C)$^{-1}$ (Tortell et al., 1996). The mesozooplankton grazing contribution to Fe regeneration was estimated based on the experimentally determined Fe regeneration during KEOPS-1 (Sarthou et al., 2008). The regeneration rates per mesozooplankton individual determined in Sarthou et al. (2008), were then multiplied by mesozooplankton abundance, calculated from the number of cells captured in a daily haul over 200 m during KEOPS-2 (Carlotti et al., 2014; values reported in Table 6 in Laurenceau et al., 2014).

BGD
11, 17861–17923, 2014

3 Results and discussion

3.1 Biogeochemical settings at our three study sites

Full descriptions of the dFe and pFe distributions can be found in Quéroué et al. (2014) and van der Merwe et al. (2014), respectively, with further presentation of the distributions of other micronutrient trace elements (Mn, Co, Ni, Cu, Cd, Pb) from KEOPS-2 to be presented elsewhere. However, briefly our subset of stations used for the iron budgets can be described as follows.

3.1.1 Reference station R-2

In the upper 100 m, we observed a salinity minimum (33.8) and temperature maximum (2.2 °C) characteristic of Antarctic surface water (AASW) overlying a layer of winter water (WW) at 180–200 m (T_{min} of 1.6 °C) (Fig. 3a). Deeper in the water column, a T_{max} of 2.5 °C at 500 m (associated with an oxygen minimum; not shown) was indicative of upper circumpolar deep water (UCDW) overlying a salinity maximum of 34.8 at 1830 m in lower circumpolar deep water (LCDW). Phytoplankton abundance was low (0.2 µg chl *a* L^{-1}; Lasbleiz et al., 2014) and dominated by diatoms, in waters with relatively high surface nitrate concentrations (> 25 µmol L^{-1}; Blain et al., 2014b), typical of Southern Ocean HNLC conditions (Lasbleiz et al., 2014).

Dissolved Fe concentrations were very low at the surface (< 0.1 nmol L^{-1}) and increased with depth averaging 0.3 nmol L^{-1} in LCDW, broadly tracking the nitrate profile. The pFe profile showed similar structure to the dFe profile, but with surface and deep water concentrations between 0.3 and 1.1 nmol L^{-1} (the deepest sample was 148 m above the seafloor). The exception was at 500 m where interestingly we observed a dFe and pFe peak of 0.4 and 1.6 nmol L^{-1}, respectively. Whilst this maximum may have arisen due to enrichment of Fe in UCDW delivered from further south, we hypothesise that the Fe supply may have originated from subsurface sediments of the nearby Leclaire Rise, a large seamount which rises to 250 m at 49°50′ S 65°00′ E (approxi-

BGD
11, 17861–17923, 2014

mately 140 km northwest of station R-2). Although the Polar Front divides the northeast flowing AASW from the eastward flowing SASW to the north (Park et al., 2008b) and in theory should restrict any enrichment from the Leclaire Rise to station R-2, similar lithogenic inputs were also observed for other dissolved (Mn; F. Quéroué, personal communication, 2014; data not shown) and particulate (Mn, Al; van der Merwe et al., 2014) trace elements.

The dFe profile at the KEOPS-2 reference station R-2 is similar to the KEOPS-1 reference station C11 (with the exception of the R-2 enrichment in the 200–700 m depth strata; Fig. 4a), noting that the location of C11 was quite different – in HNLC waters to the southeast of the Kerguelen plateau (51°39′ S, 78°00′ E) – and we had only 1 dFe data point in UCDW at C11. In contrast to the similarity of the dFe profiles, the pFe profile at C11 was generally lower than R-2, with mean values through the water column of $0.2 \pm 0.14\,\mathrm{nmol\,L^{-1}}$ (Bowie, unpublished data) compared to $0.53 \pm 0.35\,\mathrm{nmol\,L^{-1}}$ for station R-2.

3.1.2 Plateau station A3

Stations A3-1 (Fig. 3b) and A3-2 (Fig. 3c) were in relatively shallow waters on the central plateau, and were impacted by plateau sediments and possibly fluvial and glacial runoff from basaltic rocks of Heard Island ∼ 300 km upstream (van der Merwe et al., 2014; M. Grenier, personal communication, 2014). A pycnocline was observed at ∼ 190 m, above which the salinity (33.9) and nitrate (∼ 29 $\mu\mathrm{mol\,L^{-1}}$) were relatively constant. The mixed layer shoaled (from 165 to 123 m) and increased in temperature (from 1.7 to 2.2 °C) between the two visits to A3, consistent with springtime warming of surface waters. We believe the water masses at A3-1 and A3-2 are comparable since surface waters move slowly in this region (Park et al., 2008, 2014a; Zhou et al., 2014); this was confirmed by rare earth element (REE) data which indicated similar water masses at both stations marked with fresh continental supplies, only modified by biological processes (M. Grenier, personal communication, 2014).

BGD
11, 17861–17923, 2014

Surface chlorophyll images revealed that during the 28 days between the first and second visits to A3, a large diatom spring bloom developed mostly dominated by lightly silicified *Chaetoceros* spp. (surface chl *a* increasing from 0.2 $\mu g\,L^{-1}$ at A3-1 to 1.3 $\mu g\,L^{-1}$ at A3-2; Lasbleiz et al., 2014), which likely resulted in the drawdown of dFe (mean mixed layer values decreasing from 0.3–0.4 $nmol\,L^{-1}$ at A3-1 to 0.1–0.2 $nmol\,L^{-1}$ at A3-2). The peak of biomass had passed by the time we sampled at A3-2, with the bloom starting to fade (Trull et al., 2014). Below the mixed layer, similar dFe profiles were observed during both visits to A3, with expected significant increases at depth towards the plateau floor (e.g., to 1.30 $nmol\,L^{-1}$ at 480 m at A3-2; note, due to operational constraints, there was no dFe data deeper than 340 m at A3-1). Such enrichments at depth were also observed in dissolved Mn and Co profiles (F. Quéroué, personal communication, 2014; data not shown), indicative of plateau sedimentary supply.

The pFe profiles at A3 showed similar structure to the dFe profile, with lower values at the surface ($< 9\,nmol\,L^{-1}$ at A3-1 and $< 2\,nmol\,L^{-1}$ at A3-2), increasing with depth due to enrichment from bottom sediments (up to 33 and 14 $nmol\,L^{-1}$ at 440 m at A3-1 and A3-2, respectively), and were on average 10 times greater than dissolved concentrations through the water column. The mixed layer pFe concentrations changed remarkably between the two visits, and the full water column integrated pool was ~ 70 % lower at A3-2 compared to A3-1. Interestingly, this change was also associated with a shift of particles from the 1–53 µm size range to the > 53 µm size range, with the larger size class tripling in size (van der Merwe et al., 2014). The development of the large bloom between our two visits to A3, which consisted of a diatom community 50–210 µm in size (Trull et al., 2014) was likely responsible for converting the pFe within the surface mixed layer from the smaller size class to the larger size class. This may have been due to either: (i) physical aggregation of the particles onto diatom aggregates; and/or (ii) microbially-driven conversation of small lithogenic Fe (1–53 µm) to bioavailable forms (Frew et al., 2006; Planquette et al., 2011) and incorporation into the large (> 53 µm) diatoms as biogenic Fe, with potentially some fraction of these larger particles exported to depths below the mixed layer.

BGD
11, 17861–17923, 2014

The spring (October–November) KEOPS-2 Fe profiles at station A3 showed a similar structure to those from the late summer (January–February) KEOPS-1 study, with surface depletion, concentrations increasing with depth and enrichment just above the plateau seafloor (Fig. 4b). Through the water column, dFe was between 2–5 times greater during KEOPS-2 compared to KEOPS-1 and pFe was ∼ 10 times greater during KEOPS-2 (with the exception of the deepest samples). The lower values during KEOPS-1 were likely the result of biological uptake and export of Fe during the spring bloom prior to our arrival at the study site, combined with seasonal changes in the strength of the supply mechanisms to A3 (discussed in van der Merwe et al., 2014).

3.1.3 Plume E stations

The E stations within the bathymetrically trapped complex recirculation system showed similar hydrographic and nutrient distributions below the mixed layer (Fig. 3d–f), which shoaled from 64 m at E-1 to 32 m at E-3 to 39 m at E-5, with some internal variability in water column structure at mid-depths. Surface waters warmed from 2.7 to 3.4 °C between the occupations of E-1 and E-5, although no significant nitrate drawdown was observed (Blain et al., 2014b). Below AASW, a subsurface temperature minimum (T_{min}, ∼ 1.7 °C) was observed between 180 m (E-1) and 220 m (E-5), characteristic of WW. The T_{min} feature is associated with waters south of the PF, although the recirculation feature probably also received SAZ waters mixed in from the north (d'Ovidio et al., 2014). T, S and O_2 characteristics indicated the presence of UCDW (∼ 600–700 m) and LCDW (deeper than ∼ 1300 m) deeper in the water column above the seafloor (Quéroué et al., 2014). Water parcel trajectories calculated from altimetry based geostrophic currents indicated that it took generally > 2 months for Fe-rich waters from the plateau to travel to the downstream plume site associated with the recirculation feature (E stations) (d'Ovidio et al., 2014). However shorter transport times are also possible due to episodic transport across the PF (Sanial et al., 2014).

Waters at the plume stations showed the largest spatial heterogeneity in surface biomass as revealed by the evolution of the mosaic of complex blooms seen in satellite

BGD
11, 17861–17923, 2014

images (see Supplement in Trull et al., 2014). We observed moderate surface chl *a* levels ranging from 0.3–0.4 $\mu g\,L^{-1}$ at E-1 and E-3 to 0.5–0.9 $\mu g\,L^{-1}$ at E-5 (Lasbleiz et al., 2014), noting that as much as 50 % of the chlorophyll was below the mixed layer at the plume stations due to stratification of the upper water column in the warm spring conditions. Unlike the plateau bloom dominated by large cells > 53 µm, the community in the plume E stations was more mixed (Laurenceau et al., 2014), with cells present in both the 5–20 and 50–200 µm size classes (Trull et al., 2014). The E stations showed the highest C export fluxes of all regions as estimated from Th deficits, nitrate depletions, and free-drifting sediment trap observations (Planchon et al., 2014; Trull et al., 2014; Laurenceau et al., 2014).

Due to operational constraints, no dFe data was available at station E-1. The dFe vertical profiles at E-3 and E-5 were quite different, with a distinct surface enrichment to 0.4 $nmol\,L^{-1}$ at E-3 above a minimum of 0.2 $nmol\,L^{-1}$ at 100 m. This feature was absent at station E-5, where dFe was depleted to < 0.1 $nmol\,L^{-1}$ at the surface, likely due to biological Fe uptake, which was highest at E-5 (1745 $nmol\,m^{-2}\,d^{-1}$) compared to A3-2 (1120 $nmol\,m^{-2}\,d^{-1}$) (Table 1) and E-4E (880 $nmol\,m^{-2}\,d^{-1}$; data not shown), despite lower POC and primary production (see discussion below and Fourquez et al., 2014). Deeper in the water column (> 500 m) at E stations, dFe was broadly uniform (0.3–0.5 $nmol\,L^{-1}$).

The pFe distributions at the three E stations were similar with a surface (35–40 m) enrichment (1.3–1.5 $nmol\,L^{-1}$), a minimum at ∼ 100–200 m below the mixed layer (0.4–0.5 $nmol\,L^{-1}$; broadly consistent with the T_{min} layer), above a maximum at 280–600 m (1.4–2.1 $nmol\,L^{-1}$), and with evidence of enrichment near the seafloor at depths > 1800 m (up to 1.3–2.1 $nmol\,L^{-1}$). By applying biogenic (using P) and lithogenic (using Al) normalisers to the data (see "Construction of iron budgets" section below and van der Merwe et al., 2014), surface pFe enrichment was roughly equally composed of biogenic and lithogenic Fe, whilst the 300–600 m maximum was predominantly composed of lithogenic Fe (> 100 fold greater than biogenic Fe at these depths), most likely from waters enriched with Fe from sediments and transported laterally eastward off the

BGD
11, 17861–17923, 2014

Kerguelen plateau which sits at 530 m below the sea surface. There was no obvious change in pFe distributions in surface or deep waters during the bloom evolution at the pseudo-Lagrangian E stations.

The KEOPS-1 study only occupied one station in the plume east of Kerguelen (A11 at 49°09′ S 74°00′ E). Dissolved Fe at A11 ranged from 0.09 nmol L^{-1} at the surface to 0.17 nmol L^{-1} at 1500 m (Blain et al., 2008b), and pFe ranged from 0.07 nmol L^{-1} at the surface to 0.81 nmol L^{-1} at 1500 m (Andrew Bowie, unpublished data); thus much lower than our KEOPS-2 observations at the E site (noting different sampling and digestion methods for pFe were used for the two cruises).

3.2 Construction of iron budgets

The primary aim of this work was to use our observations of Fe pools and fluxes to understand the sources, sinks and biological Fe cycling, and evaluate if Fe supply could meet demand in both the high-Fe and low-Fe environments in the vicinity of the Kerguelen archipelago during the KEOPS-2 study. Iron budgets have been constructed for previous experiments in waters fertilised with Fe both naturally (Sarthou et al., 2008; Bowie et al., 2009; Ellwood et al., 2014) and artificially (Bowie et al., 2001) as well as low-Fe conditions (Price and Morel, 1998; Boyd et al., 2005). These studies have combined geochemical and chemical components to demonstrate that the dominant long-term fluxes of Fe are associated with the particulate pool (dust supply and particle export), whilst studies on Fe uptake and microbial cycling have shown that short-term fluxes within the "ferrous wheel" are dominated by biological uptake and remineralisation (Strzepek et al., 2005). Here, we follow a similar approach to that used by Bowie et al. (2009) for the SAZ-Sense study south of Tasmania (Australia) at our three study sites. Since all parameters in our iron budget calculations were only measured at stations R-2, A3-2 and E-5, discussion will focus on these stations, noting that Fe export at R-2 was estimated from Th fluxes and Fe/Th ratios (Planchon et al., 2014) since our P-trap deployment at this station was not successful. Data for stations A3-1, E-1 and

BGD
11, 17861–17923, 2014

E-3 are given to provide a context for spatial and temporal changes in the Fe pools and fluxes during KEOPS-2, and are collated in Table 1.

3.2.1 Iron pools

Iron and carbon pools were calculated by integrating the dissolved and particulate profiles down to the base of the surface mixed layer, defined as the depth where the potential density equalled the potential density at 10 m + 0.02 kg m^{-3} (Park et al., 2014a). The mixed layer varied from 165 m at station A3-1 to 32 m at station E-3, consistent with the seasonal shoaling as surface waters warmed, but remained deep (> 120 m) on the plateau throughout the study due to deep mixing as a result of several passing storms.

Integrated pools of both dissolved (~ 5×) and particulate (~ 10×) Fe were significantly greater on plateau A3 compared to the plume E, with stocks at the reference station R-2 lower still. Horizontal dFe supply from the plateau to the plume was either or both via: (i) a geostrophic path looping along the northern side of the PF and then back into the recirculation feature (d'Ovidio et al., 2014), or (ii) direct Ekman flux transport of Fe-rich coastal water across the polar front driven by westerly winds, as indicated by radium (Ra) tracers (Sanial et al., 2014). The latter process is supported by Lagrangian trajectories of water parcels derived from altimetry, which showed the polar front was not a strong barrier to water mass movement, with transport of waters across the front taking place on timescale of days-weeks but being highly variable in space and time. The pFe pool showed the same variability as the dissolved pool at our three study sites and exceeded the dFe stocks at all sites by factors of approximately 19–26 (A3), 31 (E) and 6 (R-2), although it is estimated that only ~ 2–3 % of the particulate pool could be converted into bioavailable forms by physically or biologically-mediated dissolution (Schroth et al., 2009). If we assume that station A3-1 represented pre-bloom conditions and the integrated mixed layer pool of 54 µmol dFe m^{-2} was a good estimate of the winter stock, observations show that only 4 weeks later at station A3-2, almost 60 % of the winter stock had been drawn down to 21 µmol m^{-2}. If annual variability is

BGD
11, 17861–17923, 2014

low, by late summer > 90 % of the winter stock had been used with only 4.7 µmol dFe m^{-2} remaining in the surface mixed layer at A3 (KEOPS-1 data; Blain et al., 2007).

Biogenic iron (defined as the Fe associated with living phytoplankton and phytoplankton biodetritus) was calculated by assuming that all particulate phosphorus (P) was of biogenic origin, and multiplying the mean particulate P concentration in the mixed layer at each station by a maximum intracellular Fe/P ratio of 1.9 mmol mol^{-1} for natural phytoplankton assemblages measured by Twining et al. (2004) for Fe-replete conditions. These calculations follow methods reported in Planquette et al. (2013). Lithogenic Fe was calculated by assuming that all particulate aluminium (pAl) was of lithogenic origin and by multiplying the mean pAl concentration in the mixed layer by a lithogenic Fe/Al ratio of 0.36 mol mol^{-1}, which is the mean value based on basaltic rocks from the Crozet region (0.51; Gunn et al., 1970) and crustal materials (0.2; Wedephol, 1995). A chosen Fe/Al ratio of 0.36 mol mol^{-1} is also very similar to that of 0.33 used extensively in earlier calculations (Taylor and McLennan, 1985) and reported for the deep Atlantic Ocean (Sherrell and Boyle, 1992). This approach is dependent not only on the chosen Fe/Al ratio, but also assumes that processes other than biological assimilation, such as adsorption and scavenging onto organic particles, photo-reduction, surface precipitation, and chemically and biologically driven dissolution, are not significant (Measures et al., 2008; Planquette et al., 2011, 2013; Ellwood et al., 2014). Since biogenic and lithogenic Fe were calculated independently, their sum may be less than the observed total particulate Fe concentration. This is likely due to plasticity in the chosen Fe/Al and Fe/P ratios and differential remineralisation rates for Fe, Al and P. Nevertheless, our estimates of biogenic and lithogenic Fe provide a perspective on the relative contributions to the total pFe pool.

Reference and plume waters contained roughly an equal fraction of biogenic and lithogenic Fe. The origin of this biogenic Fe pool will be a combination of biological uptake of dFe, physical adsorption onto suspended biological particles, and conversion from the lithogenic fraction (likely driven by microbes), with these processes operating on different timescales (Boyd et al., 2005; Frew et al., 2006; Planquette et al., 2011).

BGD
11, 17861–17923, 2014

On the contrary, the plateau stations contain 19–69 times more lithogenic Fe than biogenic Fe, consistent with the supply from the nearby sediments of the plateau and Heard Island. Measurement of other geochemical "fingerprint" particulate tracers (such as Al, Mn) on the plateau confirmed the provenance of Fe supplied from the Kerguelen shelf sediments in the particulate phase (van der Merwe et al., 2014).

3.2.2 Internal iron supply

Vertical fluxes were calculated as follows. A vertical diffusivity (K_z) at the base of mixed layer of $10^{-5}\,m^2\,s^{-1}$ was used for the plume and reference site, and $3 \times 10^{-4}\,m^2\,s^{-1}$ for the plateau site, estimated from the Shih parameterisations using the Thorpe scale method (Park et al., 2014b). These values are comparable to K_z values estimated for KEOPS 1 using the Osborn model ($4 \times 10^{-4}\,m^2\,s^{-1}$) (Park et al., 2008a). Vertical diffusivity was multiplied by the vertical dFe gradient for each profile, which was determined using the linear part of the vertical profiles corresponding to the 150–200 m depth strata in Fig. 3a–f, consistent with calculations for KEOPS-1 (Blain et al., 2007). Vertical diffusivity of Fe was negligible at reference and plume sites, but significant on the plateau due to both the higher vertical diffusivity and the steeper Fe gradient between 150 and 200 m.

Upwelling was defined as the vertical velocity (w_{ek}) induced by winds multiplied by the dFe concentration at 200 m, which corresponds to the depth of the remnant winter water. The magnitude of vertical velocity in this region has recently been studied by Rosso et al. (2014) who used the MIT general circulation model to examine the sensitivity of the vertical velocity to the horizontal resolution. They found clear differences in w due to the development of near surface sub-mesoscale frontal structures that only their highest resolution model was able to resolve. Rosso et al. (2014) reported vertical velocities for individual water parcels in excess of $100\,m\,d^{-1}$ in the Kerguelen region, with w_{ek} stronger in the downstream plume. Both the horizontal and vertical circulations were much weaker over the plateau since it acts as a natural barrier to the strong

BGD
11, 17861–17923, 2014

ACC fronts coming from the west. Unfortunately, no seasonal cycle was included in the model forcing. Therefore the temporal root mean square of the vertical velocity reported in Fig. 12b of Rosso et al. (2014) was used for the plateau and plume sites (w_{ek} = 0.5 and 1 m d^{-1}, respectively) and a conservative value of w_{ek} = 0.13 m d^{-1} (reported by de Baar et al., 1995 for the open Southern Ocean) was chosen for our reference station. Although w_{ek} was lower on the plateau compared to the plume, the higher dFe concentration at 200 m resulted in comparable estimates of upwelled Fe (Table 1).

Entrainment of Fe by episodic (intra-seasonal) deepening of the mixed layer has rarely been taken into account in field studies (Frants et al., 2013) due to the absence of data characterising the short term variability of the mixed layer depth, yet a recent compilation of observations (Nishioka et al., 2011; Tagliabue et al., 2014) and modelling studies (Mongin et al., 2008) suggests that entrainment could be a major vertical supply mechanism. We used more than 6000 vertical profiles of salinity and temperature collected in the regions of interest to estimate the seasonality of the mixed layer depth and its variability (Fig. S3). We derived the vertical supply of Fe by entrainment via hypotheses regarding the relation between the size of mixed layer depth excursions and their frequency (Supplement). Entrainment data based on transient deepening of the mixed layer was not available for station R-2; therefore we calculated this by multiplying the dFe concentration in winter water (which reflects the dFe concentration of the winter mixed layer) by the winter mixed layer depth (MLD) and assume this entrainment event happens once per year. "Detrainment" at R-2 was accounted for by multiplying this value by the summer-to-winter MLD ratio at each site.

In spring on KEOPS-2, entrainment was the dominant vertical Fe flux term on the plateau, delivering ~ 70 % of the total vertical supply and tripling the total vertical flux in comparison to budgets that neglect this process. At the plume and reference sites, entrainment was comparable to the upwelling flux. Vertical diffusion accounted for 4–8 % of the total vertical supply on the plateau. In contrast, the contribution from dFe entrainment was much reduced in late summer on KEOPS-1 (42 and 8.8 nmol m^{-2} d^{-1} for plateau and plume, respectively) due to the deepening and weakening of the ferri-

BGD
11, 17861–17923, 2014

cline (Fig. 4b). The relative magnitude of the total vertical Fe supply terms at the three study sites was: plateau > plume > reference (Table 1, row "d").

For the lateral fluxes, the horizontal supply at reference station R-2 was assumed to be zero since HNLC waters upstream and downstream of this station contained similar dFe and pFe concentrations; and as phytoplankton growth and biomass was low at this site, there would be little biogenic Fe exported below the mixed layer. On plateau Fe supply at station A3 was taken from the steady-state box model of Chever et al. (2010) which used the horizontal dFe gradient and current velocities from Park et al. (2008a) to calculate the lateral flux of 180 nmol m^{-2} d^{-1}. Lateral transport into the plume E stations was assumed to originate from Fe-fertilised plateau waters that were advected offshore (d'Ovidio et al., 2014). This value was estimated by assuming that horizontal stirring occurs in a Lagrangian framework, and by using altimetry-derived geostrophic velocities to determine transports across the plateau boundary. These estimates were combined with direct measurements of the dFe content of three different types of on-plateau stations to calculate the lateral flux over a 3 month supply period prior to the spring bloom; namely: (i) two coastal stations near to Kerguelen Island occupied on KEOPS-2 (stations TEW-1 and TEW-2), (ii) one coastal station close to Heard Island occupied during KEOPS-1 (station C1), and (iii) the central plateau station A3 considered here. This resulted in 5.4×10^7 mol Fe d^{-1} being injected into a plume size (defined at a threshold of > 0.3 µg chl *a* L^{-1} and identified from satellite images) of 2.5×10^{11} m^2 over 90 days in spring (full details of the calculations are contained in d'Ovidio et al., 2014). This equated to a lateral flux into the plume of 2400 nmol m^{-2} d^{-1} in the October–November period.

By combining our in-situ Fe measurements with estimated ages of the water bodies in the plume, we calculate a first order exponential scavenging removal constant between 0.041 to 0.058 d^{-1}, which equated to a residence time of 17 to 24 days, consistent with estimates based on the Fe inventory and Fe export in free-floating traps (15–79 days; Laurenceau et al., 2014). Since the total of the vertical and lateral fluxes in the plume were more than double those on the plateau, this may imply that the

BGD
11, 17861–17923, 2014

source waters supplying the plume from the northern Kerguelen Island shelves (which had a uniquely narrow T-S class in surface waters; Grenier et al., 2014) were richer in Fe than the plateau further south at A3. This is supported by observations of dFe in surface waters (1.2–1.8 nmol L^{-1}) at stations TEW-1 and TEW-2 which were close to Hillsborough Bay in waters only 86 m deep (Quéroué et al., 2014).

Considering only internal processes (diffusion, upwelling, entrainment, lateral transport) in supplying Fe to the surface mixed layer, the vertical terms dominated at the reference station, vertical terms were 6 fold greater than lateral terms on the plateau, whereas lateral advection was the dominant term in the plume (4–5 fold greater than the vertical terms). Since the particulate Fe stocks were abundant in surface waters (above the winter temperature minimum layer) and significantly higher than the dissolved pools (most notably on the plateau), it is likely that a fraction of the suspended lithogenic pFe from Heard Island or the Kerguelen plateau sediments also contributed to the internal dFe supply and fuelled biological responses. This is discussed in more detail later.

3.2.3 External iron supply

Data on atmospheric Fe fluxes through dust deposition and the solubility of Fe in the dust for all three study sites were taken from the nearby land-based sampling site "Jacky" (49°18′42.3″ S, 70°07′47.6″ E; altitude 250 m) on the Kerguelen Islands, as reported in Heimburger et al. (2012, 2013a). Mean total Fe fluxes taken over the period 24 November 2008 to 7 September 2010 were 500 ± 390 nmol m^{-2} d^{-1} (Heimburger et al., 2013a), which was comparable to the Crozet region upstream (895 nmol m^{-2} d^{-1}; Planquette et al., 2007) and the Southern Ocean sector south of Australia (288–488 nmol m^{-2} d^{-1}; Bowie et al., 2009), but greater than that estimated during the KEOPS-1 experiment by Wagener et al. (2008) (14–46 nmol m^{-2} d^{-1}). The remoteness of the Kerguelen region means it receives low quantities of atmospheric material (Heimburger et al., 2012; Wagener et al., 2008) the majority of which is crustal in origin, such as desert dust from South America, South Africa or Australia (Prospero

BGD
11, 17861–17923, 2014

et al., 2002; Mahowald, 2007; Bhattachan et al., 2012), although local anthropogenic activities, rock outcrops and exposed soil may also impact dust fluxes.

Atmospheric fluxes were dominated by wet deposition (Heimburger et al., 2012). Heimburger et al. (2013b) calculated the mean "soluble" Fe deposition flux (defined as $< 0.2\,\mu m$) using a median solubility of $82 \pm 18\,\%$ in rainwater on Kerguelen Islands (Heimburger et al., 2013b). These high solubilities were attributed to remoteness of the sampling location from dust sources resulting in strong cloud chemical processing during transport. However, the solubility of Fe dissolved in seawater at higher pH will be much lower (Schroth et al., 2009; Sedwick et al., 2007). Hence a conservative value of 10 % of Fe that is released into seawater was chosen (Baker et al., 2006; Mackie et al., 2006) for our budgets here, resulting in a soluble Fe atmospheric deposition flux to the Kerguelen region of $50\,nmol\,m^{-2}\,d^{-1}$ (Table 1, row "f"). This value was lower than the internal vertical supply on the plateau (~ 20 fold) and plume (~ 10 fold), insignificant compared to the lateral supply to the plume, but comparable to the lateral supply on the plateau. Although volcanic ash has not been considered here for atmospheric Fe supply, this term may have played an important role for primary productivity on the Kerguelen plateau during the middle Miocene climate transition (Abrajevitch et al., 2014).

3.2.4 Iron export

Downward Fe and C fluxes were measured directly in free-floating sediment P-traps at the plateau (A3-2) and plume (E-1, E-3, E-5) stations, and estimated using the ^{234}Th fluxes and Fe/Th ratios at the reference site (R-2). The sinking of pFe was by far the greatest loss term in our budgets, with $5746\,nmol\,m^{-2}\,d^{-1}$ of total Fe exported from the mixed layer on the plateau, between 895 and $4579\,nmol\,m^{-2}\,d^{-1}$ exported at the plume stations and $1302\,nmol\,m^{-2}\,d^{-1}$ exported at the reference station. The flux of sinking pFe decreased from station E-1 to E-3 to E-5 concurrent with the seasonal progression of the bloom, and indicating the mixed layer assemblages were efficiently recycling Fe under strong grazing pressure (Laurenceau et al., 2014). The downward total pFe

BGD
11, 17861–17923, 2014

fluxes were greater than the sum of the vertical, lateral and atmospheric dFe supply on the plateau, but generally less in the plume.

Aluminium was used as a normaliser to estimate the fraction of lithogenic Fe in the exported material. The percentage lithogenic fraction of total pFe exported at the E stations remained much the same at each deployment (34–39 %), whereas the lithogenic fraction was a much larger component at A3-2 (51 %), reflecting the close proximity to sources of particulate material rich in Fe. The Fe/Al ratio of exported material was higher at E stations (1.0–1.1) and on the plateau A3-2 (0.87) compared to the Fe/Al ratio of lithogenically-dominated particles (0.2; Wedepohl, 1995), confirming a significant amount of exported Fe was biogenic in origin. Interestingly, the Fe/Al export ratios were similar to those associated with suspended particles at E stations (0.9–1.2) but lower than the Fe/Al of suspended particles at A3-2 (1.2). This suggests that the biota associated with the plateau bloom at A3 were capable of efficiently recycling and retaining biogenic particulate Fe in the mixed layer (through rapid turnover to prevent aggregation and sinking) relative to lithogenic particulate Fe, which had a shorter residence time and was preferentially exported to depth. This may be due to greater ballasting of the lithogenic particles (Ellwood et al., 2014), and is consistent with other export studies which have shown that biologically-processed particles have longer residence times than lithogenic particles in the mixed layer (Lamborg et al., 2008a). Since P may be lost from exported particles much faster than Fe due to bacterial remineralisation and zooplankton consumption (Schneider et al., 2003; Lamborg et al., 2008b), it was not appropriate to apply a biogenic normaliser to the P-trap data as this may underestimate the biogenic Fe component of particles captured in the traps.

Iron export fluxes were greater during the spring study of KEOPS-2 compared to the late summer study of KEOPS-1 (Table 2). This difference between the KEOPS studies was also observed in Fe uptake rates (Fourquez et al., 2014). Such observations may be simply related to the seasonal supply; in other words, greater Fe supply in spring resulted in greater Fe uptake and export. Determined pFe sinking fluxes were also greater than the CROZEX experiment (Planquette et al., 2011), the SAZ-Sense

BGD
11, 17861–17923, 2014

expedition south of Tasmania (Bowie et al., 2009) and those observed during the Fe-Cycle I expedition east of New Zealand (Frew et al., 2006), of similar magnitude to those reported by Bowie et al. (2001) during the SOIREE iron fertilisation experiment (5.2 $\mu mol\,m^{-2}\,d^{-1}$), but much lower than Ellwood et al. (2014) reported for FeCycle II.

The export of particulate organic carbon (POC) into our P-traps followed the same trend to that of pFe at the E stations, decreasing from $7.0 \pm 2.3\,mmol\,m^{-2}\,d^{-1}$ at E-1 to $2.0 \pm 1.0\,mmol\,m^{-2}\,d^{-1}$ and E-5 (Table 1). Despite the higher pFe vertical fluxes at A3-2, POC export was lower than the E stations. The C export fluxes at 200 m at A3-2 using our P-traps (Laurenceau et al., 2014) were similar to results estimated from ^{234}Th deficits by Planchon et al. (2014; 2.3 ± 0.7 and $3.8 \pm 0.8\,mmol\,C\,m^{-2}\,d^{-1}$, respectively). Comparison of these POC fluxes to results (for the A3 plateau site only) obtained during KEOPS-1 illustrates highly dynamic variations, reflecting the rapid decline of biomass during autumn (Blain et al., 2007). Specifically, P-trap measurements of POC fluxes at 200 m during KEOPS-1 decreased from 3.7 ± 0.3 to $1.3 \pm 0.3\,mmol\,C\,m^{-2}\,d^{-1}$ over two visits to A3 in February 2005 (Trull et al., 2008), whereas estimates based on ^{234}Th at this time, reflecting the previous ~ 30 days of export, suggested much higher values ($25 \pm 7\,mmol\,C\,m^{-2}\,d^{-1}$; Savoye et al., 2008). These variations illustrate the difficulty of constraining budgets in temporally evolving systems, providing a cautionary note to our efforts. Additional discussion of temporal and spatial export flux variations during KEOPS-2 is provided in Laurenceau et al. (2014) and Planchon et al. (2014).

3.2.5 Biological iron recycling

Intracellular Fe uptake by phytoplankton and bacteria > 0.2 µm (Fourquez et al., 2014) was measured at stations A3-2 and E-5 when the bloom was rapidly growing (Cavagna et al., 2014). Iron uptake fluxes were similar on both the plateau (A3-2) and in the plume (E-5), ranging between 1120 and $1745\,nmol\,m^{-2}\,d^{-1}$. If we assume that the Fe uptake rate of $28.1\,pmol\,L^{-1}\,d^{-1}$ measured at E-5 (Fourquez et al., 2014) was conservative at E stations, $0.17\,nmol\,L^{-1}$ of Fe could have been consumed in surface waters between the occupations of stations E-4E and E-5. This is consistent with the observed

BGD
11, 17861–17923, 2014

decrease in surface dFe concentrations from 0.19 to 0.06 nmol L^{-1} at E-4E and E-5, respectively (Quéroué et al., 2014). The net and gross demand calculated at A3 during KEOPS-1 (204 and 408 nmol m^{-2} d^{-1}, respectively; Sarthou et al., 2008) is approximately 3–5 times smaller than the intracellular Fe uptake at A3-2 during KEOPS-2 for a similar C biomass (mean value of 12.7 and 10.3 µmol L^{-1} POC in surface at KEOPS-1 and KEOPS-2, respectively; Cavagna et al., 2014), perhaps indicating luxury uptake as well as important differences in community composition and activity (primary production). These studies enable opportunity to compare KEOPS-2 to KEOPS-1 data and generate a general picture of the seasonal progress from early spring to late summer, assuming that inter-annual and spatial variability is low, which may not be the case (Grenier et al., 2014).

The bacterial and mesozooplankton contributions to Fe regeneration were calculated separately (Table 3). Volumetric values varied between 0.06 and 0.59 pmol Fe L^{-1} d^{-1}, and between 0.04 and 0.08 pmol Fe L^{-1} d^{-1}, for bacterial and mesozooplankton Fe regeneration, respectively. The mesozooplankton rates were much lower than for KEOPS-1 because there were much fewer individuals (0.26–0.56 L^{-1}, compared to about 1–6 individuals L^{-1} for KEOPS-1 – see Fig. 2 in Carlotti et al., 2008). Total Fe regeneration fluxes ranged from 10 (R-2) to 71 (A3-2) nmol m^{-2} d^{-1}.

A similar Fe regeneration calculation was also performed based on the C budget by using the % of gross community production (GCP) that is remineralized for KEOPS-2 and results from Fe uptake experiments described above. This yielded higher Fe regeneration estimates in the range 1–11 pmol L^{-1} d^{-1}. Specifically, for station A3-2, 23 % of GCP was remineralised and therefore the Fe regeneration flux in the mixed layer was 1119 nmol m^{-2} d^{-1}. Similarly, for E-5, 34 % of GCP was remineralised resulting in a Fe regeneration flux of 504 nmol m^{-2} d^{-1}. Since the Fe regeneration fluxes based on the C budget are much greater (~ 16×) than those calculated using the first approach, this suggests that the remineralisation efficiency for Fe regeneration appears to be less than that of C.

BGD
11, 17861–17923, 2014

Iron regeneration fluxes can be compared with those from the KEOPS-1 study using the same first approach above. For station A3 on KEOPS-1, this resulted in a Fe regeneration flux of 1 pmol L^{-1} d^{-1} in surface waters. Malits et al. (2014) also calculated the release of bacterial bound Fe by viral lysis (0.42 pmol L^{-1} d^{-1}), which was the dominant loss term during KEOPS-1. This value compared to 1.5 pmol L^{-1} d^{-1} determined in zooplankton grazing experiments (Sarthou et al., 2008), suggesting that grazing and microbial Fe cycling were in a similar range, and the total Fe regeneration was between 2–3 pmol L^{-1} d^{-1} for KEOPS-1.

Importantly, Fe regeneration was much lower during the early compared to late bloom stage and was dominated by bacterial regeneration in spring (60–90 % of total Fe regeneration). Strezepek et al. (2005) estimated Fe regeneration rates for herbivores (16.5–18.4 pmol L^{-1} d^{-1}), bacterivores (15–25.5 pmol L^{-1} d^{-1}) and viruses (0.4–28 pmol L^{-1} d^{-1}), which is equivalent to a total Fe regeneration rate of 1435–3236 nmol m^{-2} d^{-1} for a 45 m mixed layer during FeCycle II. Bowie et al. (2009) estimated Fe regeneration to be 261–1206 nmol m^{-2} d^{-1} for the SAZ-Sense experiment. So our determined KEOPS-2 mixed layer Fe regeneration rates (71 and 31 nmol m^{-2} d^{-1} at A3-2 and E-5, respectively) were on the lower end of the range reported in other sectors of the Southern Ocean, and clearly insufficient to meet demand (measured as Fe uptake) at all stations, indicating a reliance on "new" Fe supply. This is discussed in more detail below.

3.3 Sequestration efficiencies: iron-to-carbon ratios

The mixed layer phytoplankton intracellular Fe/C uptake ratios were calculated directly from deckboard incubations for stations A3-2 (0.007 mmol mol^{-1}) and E-5 (0.021 mmol mol^{-1}) (Table 1). These values are similar to those reported for other natural and artificial iron fertilisation studies in the Southern Ocean, including for Fe-limited conditions during SOFeX (0.01 mmol mol^{-1}; Twining et al., 2004), those inside the KEOPS-1 plateau bloom (0.005 mmol mol^{-1}; Sarthou et al., 2008), but lower than those reported for SAZ-Sense (0.06–0.07 mmol mol^{-1}; Bowie et al., 2009).

BGD
11, 17861–17923, 2014

Suspended mixed layer Fe/C ratios (Table 1) were significantly higher than phytoplankton intracellular uptake ratios. This finding is consistent with the removal of C at a faster rate than that of Fe, and for Fe to be added through new sources after phytoplankton uptake. Differences may also arise because of luxury uptake, the timescale of integration in deckboard experiments compared to Fe/C ratios in ocean suspended and sinking particles (which are broadly similar – see below), and/or that our system was not in steady-state. Also, since a Ti-citrate-EDTA wash was used to remove extracellular surface Fe during the incubation experiments, but not on particles collected in the ISPs and P-traps, our suspended and sinking pFe concentrations include Fe present within cells, adsorbed to cell walls, detrital Fe and lithogenic Fe. This would tend to increase Fe/C in suspended particles. Differences between intracellular and suspended mixed layer Fe/C ratios may also derive from the C term, since the ISP sampling includes detrital material as well as living cells.

We also calculated the ratio of total particulate (biogenic + lithogenic) Fe over POC (i.e., Fe_{tot}/C) and the ratio of biogenic Fe over POC (i.e., Fe_{bio}/C) following the methods above. Suspended Fe_{tot}/C ratios (Fig. 5) were remarkably similar at all E stations and station R-2, but higher on the plateau at A3 stations (Table 1). We also observed generally surface-to-deep increases in Fe_{tot}/C ratios in suspended particles at all stations (Fig. 5), consistent with earlier findings (Frew et al., 2006). This contrasts with the decreasing Fe_{bio}/C ratios with depth, noting that a constant Fe/P was used to estimate the Fe_{bio} component. These findings indicate that Fe is preferentially retained within, and adsorbed to, sinking particles (i.e., scavenging drives the Fe_{tot}/C ratio), but biogenic Fe is recycled at a faster rate compared to C, similar to macronutrients N and P. A preferential loss of C relative to Fe_{tot} from sinking material implies that an external input of Fe is required to sustain a downward flux of carbon.

At station R-2, the Fe_{tot}/C ratio peaked at 500 m, most likely due to lithogenic particulate Fe input (and not C) from the Leclaire Rise (see above) (note this peak was not seen in the Fe_{bio}/C ratios). At E stations, the Fe_{tot}/C ratio showed maximum values in mesopelagic intermediate waters in the 600–1000 m depth range. We also believe

BGD
11, 17861–17923, 2014

this was due to the lateral transport of lithogenic particulate Fe (and not C) from the plateau (seafloor at ~ 600 m) into the plume. This is supported by the absence of this feature in the Fe_{bio}/C ratios for E stations. Fe_{tot}/C ratios in deep waters were much higher at A3 stations (26–38 mmol mol^{-1}) compared to R-2 (4 mmol mol^{-1}) and E stations (5–7 mmol mol^{-1}), indicating enrichment of lithogenic particulate Fe above the plateau. Some fraction of this lithogenic Fe will be accessible to the biota and then be incorporated into the biogenic Fe pool. This is confirmed by modification of the Fe/Al ratio (van der Merwe et al., 2014). Inclusion of the biologically available fraction of the lithogenic Fe flux is therefore required to calculate fully the yield of carbon exported per unit Fe injected, consistent with Planquette et al. (2011) and Pollard et al. (2009).

The vertical profiles of Fe_{bio}/C (Fig. 5) showed similar structure at the three study sites, with a general decreasing trend from the surface to sea floor (opposite to that of Fe_{tot}/C). Interestingly, although Fe_{tot}/C ratios varied greatly between stations (0.2–37 mmol mol^{-1}), the Fe_{bio}/C ratio fell within a narrow band (0.01–0.08 mmol mol^{-1} for all stations and depths), which encompasses the elemental ratios of Fe-replete (0.04 mmol mol^{-1}) and Fe-limited (0.01 mmol mol^{-1}) large diatoms (Sunda and Huntsman, 1995; de Baar et al., 2008). This highlights the tight coupling between Fe_{bio} and POC in the absence of new sources of Fe, and allow us to estimate the relative remineralisation efficiencies for Fe vs. C. The Fe_{bio}/C data contrast with the findings of Planquette et al. (2011) for the CROZEX experiment who observed variable Fe_{bio}/C ratios to the north of Crozet (Fe-fertilised region) which were on average much higher than those found to the south (Fe-limited region). The fraction of Fe_{bio} relative to lithogenic Fe in particles collected below the mixed layer also depends on the stage of the bloom, the nature and magnitude of supply of new lithogenic particles, and the rate of conversation from lithogenic-to-biogenic Fe (Lam et al., 2006; Frew et al., 2006; Lam and Bishop, 2008). These factors are highly variable in the Kerguelen region and this explains the wide range of Fe_{bio}/Fe_{tot} values observed during KEOPS-2.

The Fe_{tot}/C export ratio of sinking particles in our traps were similar to suspended mixed layer ratios for the E stations, but slightly higher at A3-2 (Fig. 5), possibly due

BGD
11, 17861–17923, 2014

to the sinking of recently supplied lithogenics over the plateau. Both pFe and POC export fluxes decreased during bloom development at E stations, indicating the mixed layer became more retentive for both Fe and C. This is consistent with the picture that emerges from the E time series from primary and export production estimates which show that production was moderate and matched by the moderate export during our visits (Planchon et al., 2014; Trull et al., 2014; Cavagna et al., 2014).

Since POC export fluxes during spring (KEOPS-2) were similar to late summer (KEOPS-1), but pFe export fluxes were higher in spring compared to summer (Table 2), this resulted in a generally higher carbon sequestration efficiency (lower Fe/C) during late summer, consistent with a rapidly exporting ecosystem during bloom decline. The exported particles may have been dominated by more lithogenics and much more processed in KEOPS-2 compared to KEOPS-1, where the system had already ran out of Fe. It was also expected that growing communities during KEOPS-2 would retain dFe through luxury uptake, which may also result in observed generally higher Fe/C ratios in sinking particles during the spring bloom (KEOPS-2, FeCycle-2) compared to austral summer conditions (KEOPS-1, CROZEX, FeCycle-1; Blue Water Zone; Morris and Charette, 2013) (Table 2 and Fig. 6).

Morris and Charette (2013) presented a detailed synthesis of ^{234}Th-derived POC export and dFe budgets in studies where natural iron fertilisation fuels the substantial phytoplankton blooms observed in the Southern Ocean. Where data is available to calculate the seasonal Fe/C ratios, an order of magnitude variation (0.006–0.06 mmol mol^{-1}) is observed between different Southern Ocean regions. It is likely that Fe/C ratio variations (Table 2) reflect both experimental methodologies, different calculation approaches, observational limitations and system complexities. Le Moigne et al. (2014) have also recently shown that variability on the carbon sequestration efficiency is related to the mode of Fe delivery.

BGD
11, 17861–17923, 2014

3.4 Iron supply vs. demand

Using calculated flux estimates, a comparison of Fe supply and demand at the three sites around the Kerguelen archipelago in spring was possible (Fig. 7). In our short-term iron biogeochemical budgets, the total dFe supply from "new" sources (calculated as the sum of diffusion, upwelling, vertical and lateral advection, and atmospheric dust) to surface waters of the plume was more than twice that above the plateau and > 20 times greater than at the reference station (Table 1). The Fe demand (measured by cellular Fe uptake) in the plume was similar (1.5 times greater) to the plateau but > 40 times greater than at the reference station. "New" Fe supply was 14–94 times greater than "recycled" Fe supply ("iron remineralisation"; row "i" in Table 1) from bacterial regeneration and zooplankton grazing. This contrasts with the findings of Bowie et al. (2009) for the SAZ-Sense experiment who reported recycled fluxes that were broadly comparable with new Fe supply in the SAZ in summer at study sites further from natural iron fertilisation.

Since Fe supply from "new" sources was greater than the Fe demand (uptake minus remineralisation as a "recycled" Fe source) at all stations (R-2, A3-2 and E-5), this resulted in a positive value for row "k" in Table 1 (i.e., there was no additional Fe required to balance the dissolved budget). This finding is consistent with other observations at both the plateau and plume sites which were Fe replete in early spring, but somewhat surprising for the HNLC reference site R-2. This may partly be a result of an overestimate of the atmospheric supply used in calculations presented here from literature data. Another explanation is that the parameters used in our "short-term" iron budget calculations are decoupled in time (e.g., there will be an offset between the mechanisms for organism acquisition of Fe and the processes resulting in Fe-laden particles leaving the upper ocean), and the short-term Fe budget is based on an "instantaneous picture" of different fluxes that were not in steady-state.

Interestingly, at station A3-2, the sink processes (Fe export and uptake) are so large and the regenerated Fe flux small that the total (dissolved + particulate) Fe losses are

BGD
11, 17861–17923, 2014

far greater than the net dFe supply (Fig. 7a). In other words, to a first order the budget is not balanced with known sources of Fe insufficient to account for the downward flux, even if we only accounted for the non-lithogenic particulate Fe export flux (row "I" in Table 1). This implies there is a missing flux term in the budget at A3 and this is likely lithogenic pFe from the Kerguelen plateau and/or Heard Island (and this may be converted to biogenic Fe). Currently, we do not invoke a lithogenic pFe to dFe transfer in the budget, which could increase the Fe supply on the plateau significantly, although at present we do not know what fraction of particulate material is converted into the dissolved form. This will vary largely with the mineralogy (Schroth et al., 2009), provenance of the particles, and seawater characteristics (e.g., organic complexation; Shaked et al., 2012). By applying a solubility of 2.5 % used for KEOPS-1 at A3 to enable Fe supply to meet demand (Blain et al., 2007), this would provide an extra 10–34 $\mu mol\,m^{-2}$ of dFe to the mixed layer, approximately doubling the dFe standing stock; these values are comparable to our observations and suggest that particulate material plays a major role in the supply of dFe (van der Merwe et al., 2014). Further, if we assume pFe from glacial melt is delivered over a 3 month period, this would provide an additional 111–387 $nmol\,m^{-2}\,d^{-1}$ to the mixed layer at A3, values of similar magnitude to the individual vertical and lateral supply terms. Whilst a dissolution estimate of 2.5 % may be considered to be at the upper extent of the range, Schroth et al. (2009) have reported that 2–3 % of Fe is soluble in glacial flour which can remain suspended in surface water for several months after delivery from Kerguelen Island (van der Merwe et al., 2014).

The release of Fe to biota via conversion of lithogenic to biogenic Fe has been previously suggested (Lam et al., 2006; Frew et al., 2006; Borer et al., 2009; Planquette et al., 2011) and the present work strongly supports this hypothesis, with our data (Fig. 5) indicating that biogenic Fe has a longer residence time in the upper ocean than lithogenic Fe which is not accessed by biota. The role of pFe in supplying bioavailable Fe is also supported by the similarity of the pFe and dFe profile shapes in Fig. 3, which

BGD
11, 17861–17923, 2014

infer that pFe may be contributing to the control of dFe, either by supplying it or because biogenic particles are controlling both.

Finally, our estimation of Fe supply and regeneration allowed us to estimate an *fe* ratio, defined by Boyd et al. (2005) as *fe* = uptake of new/uptake of new + regenerated Fe, for the plume region of 1.4. This was higher than the *fe* ratio calculated for KEOPS-1 (0.49; Sarthou et al., 2008), which at that time was comparable to the average *f* ratio (corresponding to NO_3^- uptake/(NO_3^- uptake + NH_4^+ uptake)) for nitrogen (0.41; Mosseri et al., 2008), indicating that both NH_4^+ and regenerated Fe could support export production. Conversely, the KEOPS-2 *f* ratio was higher (up to 0.9; Cavagna et al., 2014), indicating that primary production was mainly sustained by nitrate uptake. The *fe* ratios for both KEOPS studies were much higher than the *fe* ratio estimated during FeCycle (0.17, Boyd et al., 2005) and SAZ-Sense (0.06–0.16; Bowie et al., 2009). This confirms that in the Kerguelen region, there are sufficient "new" sources of Fe delivered on a seasonal timescale (predominantly via intra-seasonal entrainment, winter mixing, lateral transport and particulate Fe dissolution) available to sustain the massive bloom observed in spring.

4 Conclusions

The complex regional circulation, multiple sources and transport pathways of iron above and downstream of the naturally fertilised Kerguelen plateau region results in a mosaic of phytoplankton blooms. The budgets presented here result from direct measurements of the Fe inventories and fluxes between different pools. The system was not in steady-state during the period of the KEOPS-2 observations, and the exchange of Fe between the dissolved, biogenic and lithogenic pools was highly dynamic in time and space. Our analysis highlights the important role of pFe, the inherent heterogeneity and biogeochemical differences associated with particulates within and exported below the mixed layer, and the lithogenic to biogenic conversion pathways.

BGD
11, 17861–17923, 2014

This study also highlights the significance not only of the mode of Fe fertilisation on the plateau (predominantly vertical) vs. the plume (predominantly lateral), but also of the relative magnitude. Importantly, since the Fe supply from "new" sources to the plume was more than double that above the plateau, this implies the waters that supply the plume are not the same as those at A3 station on the southern plateau, and the plume must be supplied with water from the northern part of the plateau or Kerguelen coastal waters, which are richer in dFe (Quéroué et al., 2014; Trull et al., 2014). This source of Fe, which will contain a large fraction of particulate material (van der Merwe et al., 2014) that is transported off the Kerguelen plateau, is therefore an important but previously unquantified contribution to the downward flux of Fe exiting the upper ocean in the plume. Moreover, the KEOPS-2 results are tightly linked to the mode of Fe supply that is different from dust deposition or purposeful additions, and to the concomitant supply of major nutrients, and this has consequences for the carbon sequestration efficiency of the system. When Fe supply is predominantly vertical (as it is at station A3), then the C sequestration efficiency is lower (i.e., higher Fe/C) as C would be re-supplied to the mixed layer as well as Fe. This coupling has important implications in the context of different geoengineering schemes to increase the supply of Fe to surface waters.

Future efforts should focus on the quantification of the full seasonal cycle of Fe delivery, which will be fundamental to closing the iron budget around the Kerguelen archipelago over annual timescales. This will allow assessment of the important longer-term climatic and ecosystem implications with changes in the nature and strength of Fe supply with physical (weakening overturning circulation, increased stratification), and chemical (ocean acidification, warming, deoxygenation) environmental forcings, together with increases in glacial melt, rainfall and dust deposition on a warming planet.

The Supplement related to this article is available online at doi:10.5194/bgd-11-17861-2014-supplement.

BGD
11, 17861–17923, 2014

Author contributions. A. R. Bowie designed the iron budgets, performed the calculations and prepared the manuscript with contributions from all co-authors. P. van der Merve, F. Queroue, G. Sarthou, F. Chever and A. T. Townsend were responsible for trace metal sampling, analyses and data interpretation, M. Fourquez and I. Obernosterer for biological cycling, T. Trull for carbon dynamics and the P-trap deployments, F. Planchon for Th-based export, and J.-B. Sallée for vertical flux estimates. S. Blain designed the overall KEOPS-2 experiment and helped with budget calculations.

Acknowledgements. We thank the captain B. Lassiette, officers and crew of M.D. *Marion Dufresne*, Pierre Sangiardi (Institut Paul Emile Victor) and the Institut National des Sciences de l'Univers for voyage logistics and their support of the science, and voyage leader Bernard Quéguiner (Institut Mediterraneen d'Oceanologie) and chief scientist Stéphane Blain (LOMIC, Université Pierre et Marie) for leading the KEOPS-2 expedition. We acknowledge Thomas Rodemann (UTAS) for CHN analysis in the Central Science Laboratory, together with members of the ISP and P-trap teams for support at sea. Access to ICP-MS was provided through Australian Research Council LIEF funds (LE0989539). The altimeter and colour/temperature products for the Kerguelen area were produced by Ssalto/Duacs and CLS with support from CNES, and kindly prepared by Emmanuel Laurenceau (UTAS) and Francesco d'Ovidio (LOCEAN – IPSL, Université Pierre et Marie Curie). The Australian participation in the project was supported by the Antarctic Climate and Ecosystems Cooperative Research Centre and a University of Tasmania "Rising Stars" award to the lead author.

References

Abrajevitch, A., Roberts, A. P., and Kodama, K.: Volcanic iron fertilization of primary productivity at Kerguelen Plateau, Southern Ocean, through the Middle Miocene Climate Transition, Palaeogeogr. Palaeocl., 410, 1–13, doi:10.1016/j.palaeo.2014.05.028, 2014.

Assmy, P. et al.: Thick-shelled, grazer-protected diatoms decouple ocean carbon and silicon cycles in the iron-limited Antarctic Circumpolar Current, P. Natl. Acad. Sci. USA, 110, 20633–20638, doi:10.1073/pnas.1309345110, 2013.

Baker, A. R., Jickells, T. D., Witt, M., and Linge, K. L.: Trends in the solubility of iron, aluminium, manganese and phosphorus in aerosol collected over the Atlantic Ocean, Mar. Chem., 98, 43–58, doi:10.1016/j.marchem.2005.06.004, 2006.

BGD
11, 17861–17923, 2014

Bhattachan, A., D'Odorico, P., Baddock, M. C., Zobeck, T. M., Okin, G. S., and Cassar, N.: The Southern Kalahari: a potential new dust source in the Southern Hemisphere?, Environ. Res. Lett., 7, 1–7, doi:10.1088/1748-9326/7/2/024001, 2012.

Bishop, J. K. B., Lam, P. J., and Wood, T. J.: Getting good particles: accurate sampling of particles by large volume in-situ filtration, Limnol. Oceanogr.-Meth., 10, 681–710, doi:10.4319/lom.2012.10.681, 2012.

Blain, S. et al.: Effect of natural iron fertilization on carbon sequestration in the Southern Ocean, Nature, 446, 1070–1074, doi:10.1038/nature05700, 2007.

Blain, S., Quéguiner, B., and Trull, T.: The natural iron fertilization experiment KEOPS (KErguelen Ocean and Plateau compared Study): an overview, Deep-Sea Res. Pt. II, 55, 559–565, doi:10.1016/j.dsr2.2008.01.002, 2008a.

Blain, S., Sarthou, G., and Laan, P.: Distribution of dissolved iron during the natural iron-fertilization experiment KEOPS (Kerguelen Plateau, Southern Ocean), Deep-Sea Res. Pt. II, 55, 594–605, doi:10.1016/j.dsr2.2007.12.028, 2008b.

Blain, S. et al.: KEOPS-2: implementation and overview, Biogeosciences Discuss., submitted, 2014a.

Blain, S., Capparos, J., Guéneuguès, A., Obernosterer, I., and Oriol, L.: Distributions and stoichiometry of dissolved nitrogen and phosphorus in the iron fertilized region near Kerguelen (Southern Ocean), Biogeosciences Discuss., 11, 9949–9977, doi:10.5194/bgd-11-9949-2014, 2014b.

Borer, P., Sulzberger, B., Hug, S. J., Kraemer, S. M., and Kretzschmar, R.: Photoreductive dissolution of iron(III) (hydr)oxides in the absence and presence of organic ligands: experimental studies and kinetic modelling, Environ. Sci. Technol., 43, 1864–1870, doi:10.1021/es801352k, 2009.

Bowie, A. R. and Lohan, M. C.: Analysis of iron in seawater, chapter 12, in: "Practical Guidelines for the Analysis of Seawater", edited by: Wurl, O., Taylor and Francis, Boca Raton, USA, ISBN 978-1-4200-7306-5, doi:10.1201/9781420073072.ch12, 235–257, 2009.

Bowie, A. R., Maldonado, M. T., Frew, R. D., Croot, P. L., Achterberg, E. P., Mantoura, R. F. C., Worsfold, P. J., Law, C. S., and Boyd, P. W.: The fate of added iron during a mesoscale fertilisation experiment in the Southern Ocean, Deep-Sea Res. Pt. II, 48, 2703–2743, doi:10.1016/S0967-0645(01)00015-7, 2001.

Bowie, A. R., Lannuzel, D., Remenyi, T. A., Wagener, T., Lam, P. J., Boyd, P. W., Guieu, C., Townsend, A. T., and Trull, T. W.: Biogeochemical iron budgets of the Southern Ocean south

BGD
11, 17861–17923, 2014

of Australia: decoupling of iron and nutrient cycles in the subantarctic zone by the summertime supply, Global Biogeochem. Cy., 23, GB4034, doi:10.1029/2009GB003500, 2009.
Bowie, A. R., Townsend, A. T., Lannuzel, D., Remenyi, T., and van der Merwe, P.: Modern sampling and analytical methods for the determination of trace elements in marine particulate material using magnetic sector ICP-MS, Anal. Chim. Acta, 676, 15–27, doi:10.1016/j.aca.2010.07.037, 2010
Boyd, P. W. and Ellwood, M. J.: The biogeochemical cycle of iron in the ocean, Nat. Geosci., 3, 675–682, doi:10.1038/ngeo964, 2010.
Boyd, P. W., Watson, A. J., Law, C. S., Abraham, E. R., Trull, T., Murdoch, R., Bakker, D. C. E., Bowie, A. R., Buesseler, K. O., Chang, H., Charette, M., Croot, P., Downing, K., Frew, R., Gall, M., Hadfield, M., Hall, J., Harvey, M., Jameson, G., LaRoche, J., Liddicoat,M., Ling, R., Maldonado, M. T., McKay, R. M., Nodder, S., Pickmere, S., Pridmore, R., Rintoul, S., Safi, K., Sutton, P., Strzepek, R., Tanneberger, K., Turner, S., Waite, A., and Zeldis, J.: A mesoscale phytoplankton bloom in the polar Southern Ocean stimulated by iron fertilization, Nature, 407, 695–702, doi:10.1038/35037500, 2000.
Boyd, P. W. et al.: FeCycle: attempting an iron biogeochemical budget from a mesoscale SF6 tracer experiment in unperturbed low iron waters, Global Biogeochem. Cy., 19, GB4S20, doi:10.1029/2005GB002494, 2005.
Boyd, P. W. et al.: Mesoscale Iron Enrichment Experiments 1993–2005: synthesis and future directions, Science, 315, 612–617, doi:10.1126/science.1131669, 2007.
Breitbarth, E., Achterberg, E. P., Ardelan, M. V., Baker, A. R., Bucciarelli, E., Chever, F., Croot, P. L., Duggen, S., Gledhill, M., Hassellöv, M., Hassler, C., Hoffmann, L. J., Hunter, K. A., Hutchins, D. A., Ingri, J., Jickells, T., Lohan, M. C., Nielsdóttir, M. C., Sarthou, G., Schoemann, V., Trapp, J. M., Turner, D. R., and Ye, Y.: Iron biogeochemistry across marine systems – progress from the past decade, Biogeosciences, 7, 1075–1097, doi:10.5194/bg-7-1075-2010, 2010.
Carlotti, F., Thibault-Botha, D., Nowaczyk, A., and Lefèvre, D.: Zooplankton community structure, biomass and role in carbon fluxes during the second half of a phytoplankton bloom in the eastern sector of the Kerguelen shelf (January–February 2005), Deep-Sea Res. Pt. II, 55, 720–733, doi:10.1016/j.dsr2.2007.12.010, 2008.
Carlotti, F., Jouandet, M.-P., Nowaczyk, A., Harmelin-Vivien, M., Lefèvre, D., Guillou, G., Zhu, Y., and Zhou, M.: Mesozooplankton structure and functioning during the onset of the Kerguelen Bloom during KEOPS-2 survey, Biogeosciences Discuss., submitted, 2014.

BGD
11, 17861–17923, 2014

Cavagna, A. J., Fripiat, F., Elskens, M., Dehairs, F., Mangion, P., Chirurgien, L., Closset, I., Lasbleiz, M., Flores-Leiva, L., Cardinal, D., Leblanc, K., Fernandez, C., Lefèvre, D., Oriol, L., and Quéguiner, B.: Biological productivity regime and associated N cycling in the surface waters over and downstream the Kerguelen Island area, Southern Ocean, Biogeosciences Discuss., submitted, 2014.

Chever, F., Sarthou, G., Bucciarelli, E., Blain, S., and Bowie, A. R.: An iron budget during the natural iron fertilisation experiment KEOPS (Kerguelen Islands, Southern Ocean), Biogeosciences, 7, 455–468, doi:10.5194/bg-7-455-2010, 2010.

Christaki, U., Lefèvre, D., Georges, C., Colombet, J., Catala, P., Courties, C., Sime-Ngando, T., Blain, S., and Obernosterer, I.: Microbial food web dynamics during spring phytoplankton blooms in the naturally iron-fertilized Kerguelen area (Southern Ocean), Biogeosciences Discuss., 11, 6985–7028, doi:10.5194/bgd-11-6985-2014, 2014.

Cullen, J. T., Chong, M., and Lanson, D.: British Columbian continental shelf as a source of dissolved iron to the subarctic northeast Pacific Ocean, Global Biogeochem. Cy., 23, GB4012, doi:10.1029/2008GB003326, 2009.

Cutter, G. A. and Bruland, K. W.: Rapid and noncontaminating sampling system for trace elements in global ocean surveys, Limnol. Oceanogr.-Meth., 10, 425–436, doi:10.4319/lom.2012.10.425, 2012.

de Baar, H. J. W., de Jong, J. T. M., Bakker, D. C. E., Löscher, B. M., Veth, C., Bathmann, U., and Smetacek, V.: Importance of iron for plankton blooms and carbon dioxide drawdown in the Southern Ocean, Nature, 373, 412–415, doi:10.1038/373412a0, 1995.

de Baar, H. J. W. et al.: Synthesis of iron fertilization experiments: from the iron age in the age of enlightenment, J. Geophys. Res., 110, C09S16, doi:10.1029/2004JC002601, 2005.

de Baar, H. J. W. et al.: Efficiency of carbon removal per added iron in ocean iron fertilization, Mar. Ecol.-Prog. Ser., 364, 269–282, doi:10.3354/meps07548, 2008.

de Jong, J. T. M. et al.: Dissolved iron at sub-nanomolar levels in the Southern Ocean as determined by ship-board analysis, Anal. Chim. Acta, 377, 113–124, doi:10.1016/S0003-2670(98)00427-9, 2008.

de Jong, J. T. M., Schoemann, V., Lannuzel, D., Croot, P., de Baar, H., and Tison, J.-L.: Natural iron fertilization of the Atlantic sector of the Southern Ocean by continental shelf sources of the Antarctic Peninsula, J. Geophys. Res., 117, G01029, doi:10.1029/2011JG001679, 2012.

d'Ovidio, F., Della Penna, A., Trull, T. W., Nencioli, F., Pujol, I., Rio, M.-H., Park, Y.-H., Cotté, C., Zhou, M., and Blain, S.: The biogeochemical structuring role of horizontal stirring: Lagrangian

BGD
11, 17861–17923, 2014

perspectives on iron delivery downstream of the Kerguelen plateau, Biogeosciences Discuss., submitted, 2014.
Ellwood, M. J., Nodder, S. D., Boyd, P. W., King, A. L., Hutchins, D. A., and Wilhelm, S. W.: Pelagic iron cycling during the subtropical spring bloom, east of New Zealand, Mar. Chem., 160, 18–33, doi:10.1016/j.marchem.2014.01.004, 2014.
Fourquez, M., Obernosterer, I., Davies, D. M., Trull, T. W., and Blain, S.: Microbial iron uptake in the naturally fertilized waters in the vicinity of Kerguelen Islands: phytoplankton–bacteria interactions, Biogeosciences Discuss., 11, 15053–15086, doi:10.5194/bgd-11-15053-2014, 2014.
Frants, M. et al.: Analysis of horizontal and vertical processes contributing to natural iron supply in the mixed layer in southern Drake Passage, Deep-Sea Res. Pt. II, 90, 68–76, doi:10.1016/j.dsr2.2012.06.001, 2013.
Frew, R. D., Hutchins, D. A., Nodder, S., Sanudo-Wilhelmy, S., Tovar-Sanchez, A., Leblanc, K., Hare, C. E., and Boyd, P. W.: Particulate iron dynamics during FeCycle in subantarctic waters southeast of New Zealand, Global Biogeochem. Cy., 20, GB1S93, doi:10.1029/2005GB002558, 2006.
Gerringa, L. J. A., Blain, S., Laan, P., Sarthou, G., Veldhuis, M. J. W., Brussaard, C. P. D., Viollier, E., and Timmermans, K. R.: Fe-binding dissolved organic ligands near the Kerguelen Archipelago in the Southern Ocean (Indian sector), Deep-Sea Res. Pt. II, 55, 606–621, doi:10.1016/j.dsr2.2007.12.007, 2008.
Grenier, M., Della Penna, A., Thresher, A., and Trull, T. W.: Autonomous profiling float observations of the high biomass plume downstream of the Kerguelen plateau in the Southern Ocean, Biogeosciences Discuss., submitted, 2014.
Gunn, B. M., Coyyll, R., Watkins, N. D., Abranson, C. E., and Nougier, J.:, Geochemistry of an oceanite–ankaramite–basalt suite from East Island, Crozet Archipelago, Contrib. Mineral. Petr., 28, 319–339, doi:10.1007/BF00388954, 1970.
Heimburger, A., Losno, R., Triquet, S., Dulac, F., and Mahowald, N.: Direct measurements of atmospheric iron, cobalt, and aluminum-derived dust deposition at Kerguelen Islands, Global Biogeochem. Cy., 26, GB4016, doi:10.1029/2012GB004301, 2012.
Heimburger, A., Losno, R., Triquet, S., and Bon Nguyen, E.: Atmospheric deposition fluxes of 26 elements over the Southern Indian Ocean: time series on Kerguelen and Crozet Islands, Global Biogeochem. Cy., 27, 440–449, doi:10.1002/gbc.20043, 2013a.

BGD
11, 17861–17923, 2014

Heimburger, A., Losno, R., and Triquet, S.: Solubility of iron and other trace elements in rainwater collected on the Kerguelen Islands (South Indian Ocean), Biogeosciences, 10, 6617–6628, doi:10.5194/bg-10-6617-2013, 2013b.
Homoky, W. B., John, S. G., Conway, T. M., and Mills, R. A.: Distinct iron isotopic signatures and supply from marine sediment dissolution, Nat. Comm., 4, 2143, doi:10.1038/ncomms3143, 2013.
Hudson, R. J. M. and Morel, F. M. M.: Distinguishing between extra- and intracellular iron in marine phytoplankton, Limnol. Oceanogr., 34, 1113-l120, doi:10.4319/lo.1989.34.6.1113, 1989.
Johnson, K. et al.: Developing standards for dissolved iron in seawater, EOS T. Am. Geophys. Un., 88, 131–132, doi:10.1029/2007EO110003, 2007.
King, P. et al.: Analysis of total and organic carbon and total nitrogen in settling oceanic particles and a marine sediment: an interlaboratory comparison, Mar. Chem., 60, 203–216, doi:10.1016/S0304-4203(97)00106-0, 1998.
Lam, P. J. and Bishop, J. K. B.: The continental margin is a key source of iron to the HNLC North Pacific Ocean, Geophys. Res. Lett., 35, L07608, doi:10.1029/2008GL033294, 2008.
Lam, P. J., Bishop, J. K. B., Henning, C. C., Marcus, M. A., Waychunas, G. A., and Fung, I. Y.: Wintertime phytoplankton bloom in the subarctic Pacific supported by continental margin iron, Global Biogeochem. Cy., 20, GB1006, doi:10.1029/2005GB002557, 2006.
Lamborg, C. H., Buesseler, K. O., and Lam, P. J.: Sinking fluxes of minor and trace elements in the North Pacific Ocean measured during the VERTIGO program, Deep-Sea Res. Pt. II, 55, 1564–1577, doi:10.1016/j.dsr2.2008.04.012, 2008a.
Lamborg, C. H., Buesseler, K. O., Valdes, J., Bertrand, C. H., Bidigare, R., Manganini, S., Pike, S., Steinberg, D., Trull, T., and Wilson, S.: The flux of bio- and lithogenic material associated with sinking particles in the mesopelagic "Twilight Zone" of the northwest and north central Pacific Ocean, Deep-Sea Res. Pt. II, 55, 1540–1563, doi:10.1016/j.dsr1012.2008.1004.1011, 2008b.
Lasbleiz, M., Leblanc, K., Blain, S., Ras, J., Cornet-Barthaux, V., Hélias Nunige, S., and Quéguiner, B.: Pigments, elemental composition (C, N, P, and Si), and stoichiometry of particulate matter in the naturally iron fertilized region of Kerguelen in the Southern Ocean, Biogeosciences, 11, 5931–5955, doi:10.5194/bg-11-5931-2014, 2014.
Laurenceau, E. C., Trull, T. W., Davies, D. M., Bray, S. G., Doran, J., Planchon, F., Carlotti, F., Jouandet, M.-P., Cavagna, A.-J., Waite, A. M., and Blain, S.: The relative importance of phytoplankton aggregates and zooplankton fecal pellets to carbon export: insights from

BGD
11, 17861–17923, 2014

free-drifting sediment trap deployments in naturally iron-fertilised waters near the Kerguelen plateau, Biogeosciences Discuss., 11, 13623–13673, doi:10.5194/bgd-11-13623-2014, 2014.

Le Moigne, F. A. C, Moore, C. M., Sanders, R. J., Villa-Alfageme, M., Steigenberger, S., and Achterberg, E. P.: Sequestration efficiency in the iron limited North Atlantic: implications for iron supply mode to fertilized blooms, Geophys. Res. Lett., 41, 4619–4627, doi:10.1002/2014GL060308, 2014.

Mackie, D. S., Peat, J. M., McTainsh, G. H., Boyd, P. W., and Hunter, K. A.: Soil abrasion and eolian dust production: implications for iron partitioning and solubility, Geochem. Geophy. Geosy., 7, Q12Q03, doi:10.1029/2006GC001404, 2006.

Mackie, D. S., Boyd, P. W., McTainsh, G. H., Tindale, N. W., Westberry, T. K., and Hunter, K. A.: Biogeochemistry of iron in Australian dust: from eolian uplift to marine uptake, Geochem. Geophy. Geosy., 9, Q03Q08, doi:10.1029/2007GC001813, 2008.

Mahowald, N. M.: Anthropocene changes in desert area: sensitivity to climate model predictions, Geophys. Res. Lett., 34, L18817, doi:10.1029/2007GL030472, 2007.

Malits, A., Christaki, U., Obernosterer, I., and Weinbauer, M. G.: Enhanced viral production and virus-mediated mortality of bacterioplankton in a natural iron-fertilized bloom event above the Kerguelen Plateau, Biogeosciences Discuss., 11, 10827–10862, doi:10.5194/bgd-11-10827-2014, 2014.

Marsay, C. M., Sedwick, P. N., Dinninman, M. S., Barrett, P. M., Mack, S. L., and McGillicuddy Jr, D. J.: Estimating the benthic efflux of dissolved iron on the Ross Sea continental shelf, Geophys. Res. Lett., 41, 7576–7583, doi:10.1002/2014GL061684, 2014.

Martin, J. H.: Glacial–interglacial CO_2 change: the iron hypothesis, Paleoceanography, 5, 1–13, doi:10.1029/PA005i001p00001, 1990.

Measures, C. I., Landing, W. M., Brown, M. T., and Buck, C. S.: High-resolution Al and Fe data from the Atlantic Ocean CLIVAR-CO2 Repeat Hydrography A16N transect: extensive linkages between atmospheric dust and upper ocean geochemistry, Global Biogeochem. Cy., 22, GB1005, doi:10.1029/2007GB003042, 2008.

Mongin, M., Molina, E., and Trull, T. W.: Seasonality and scale of the Kerguelen plateau phytoplankton bloom: a remote sensing and modeling analysis of the influence of natural iron fertilization in the Southern Ocean, Deep-Sea Res. Pt. II, 55(5–7): 880, doi:10.1016/j.dsr2.2007.12.039, 2008.

BGD
11, 17861–17923, 2014

Moore, C. M., Hickman, A. E., Poulton, A. J., Seeyave, S., and Lucas, M. I.: Iron-light interactions during the CROZet natural iron bloom and EXport experiment (CROZEX) II: taxonomic responses and elemental stoichiometry, Deep-Sea Res. Pt. II, 54, 2066–2084, doi:10.1016/j.dsr2.2007.06.015, 2008.

Moore, J. K. and Doney, S. C.: Iron availability limits the ocean nitrogen inventory stabilizing feedbacks between marine denitrification and nitrogen fixation, Global Biogeochem. Cy., 21, GB2001, doi:10.1029/2006GB002762, 2007.

Morris, P. J. and Charette, M. A.: A synthesis of upper ocean carbon and dissolved iron budgets for Southern Ocean natural iron fertilisation studies, Deep-Sea Res. Pt. II, 90, 147–157, doi:10.1016/j.dsr2.2013.02.001, 2013.

Mosseri, J., Quéguiner, B., Armand, L., and Cornet-Barthaux, V.: Impact of iron on silicon utilization by diatoms in the Southern Ocean: a case study of Si/N cycle decoupling in a naturally iron-enriched area, Deep-Sea Res. Pt. II, 55, 801–819, doi:10.1016/j.dsr2.2007.12.003, 2008.

Nishioka, J., Ono, T., Saito, H., Sakaoka, K., and Yoshimura, T.: Oceanic iron supply mechanisms which support the spring diatom bloom in the Oyashio region, western subarctic Pacific, J. Geophys. Res., 116, C02021, doi:10.1029/2010JC006321, 2011.

Obata, H., Karatani, H., and Nakayama, E.: Automated determination of iron in seawater by chelating resin concentration and chemiluminescence detection, Anal. Chem., 5, 1524–1528, doi:10.1021/ac00059a007, 1993.

Park, Y.-H., Fuda, J.-L., Durand, I., and Naveira Garabato, A. C.: Internal tides and vertical mixing over the Kerguelen Plateau, Deep-Sea Res. Pt. II, 55, 582–593, doi:10.1016/j.dsr2.2007.12.027, 2008a.

Park, Y.-H., Roquet, F., Durand, I., and Fuda, J.-L.: Large-scale circulation over and around the Northern Kerguelen Plateau, Deep-Sea Res. Pt. II, 55, 566–581, doi:10.1016/j.dsr2.2007.12.030, 2008b.

Park, Y.-H., Durand, I., Kestenare, E., Rougier, G., Zhou, M., d'Ovidio, F., Cotté, C., and Lee, J.-H.: Polar Front around the Kerguelen Islands: an up-to-date determination and associated circulation of surface/subsurface waters, J. Geophys. Res.-Oceans, 119, 6575–6592, doi:10.1002/2014JC010061, 2014a.

Park, Y.-H., Lee, J.-H., Durand, I., and Hong, C.-S.: Validation of the Thorpe scale-derived vertical diffusivities against microstructure measurements in the Kerguelen region, Biogeosciences Discuss., 11, 12137–12157, doi:10.5194/bgd-11-12137-2014, 2014b.

BGD
11, 17861–17923, 2014

Planchon, F., Ballas, D., Cavagna, A.-J., Bowie, A. R., Davies, D., Trull, T., Laurenceau, E., Van Der Merwe, P., and Dehairs, F.: Carbon export in the naturally iron-fertilized Kerguelen area of the Southern Ocean based on the ^{234}Th approach, Biogeosciences Discuss., 11, 15991–16032, doi:10.5194/bgd-11-15991-2014, 2014.

Planquette, H. and Sherrell, R. M.: Sampling for particulate trace element determination using water sampling bottles: methodology and comparison to in situ pumps, Limnol. Oceanogr.-Meth., 10, 367–388, doi:10.4319/lom.2012.10.367, 2012.

Planquette, H. et al.: Dissolved iron in the vicinity of the Crozet Islands, Southern Ocean, Deep-Sea Res. Pt. II, 54, 1999–2019, doi:10.1016/j.dsr2.2007.06.019, 2007.

Planquette, H., Fones, G. R., Statham, P. J., and Morris, P. J.: Origin of iron and aluminium in large particles (> 53 µm) in the Crozet region, Southern Ocean, Mar. Chem., 115, 31–42, doi:10.1016/j.marchem.2009.06.002, 2009.

Planquette, H., Sanders, R. R., Statham, P. J., Morris, P. J., and Fones, G. R.: Fluxes of particulate iron from the upper ocean around the Crozet Islands: a naturally iron-fertilized environment in the Southern Ocean, Global Biogeochem. Cy., 25, GB2011, doi:10.1029/2010GB003789, 2011.

Planquette, H., Sherrell, R. M., Stammerjohn, S., and Field, M. P.: Particulate iron delivery to the water column of the Amundsen Sea, Antarctica, Mar. Chem., 153, 15–30, doi:10.1016/j.marchem.2013.04.006, 2013.

Pollard, R. T. et al.: Southern Ocean deep-water carbon export enhanced by natural iron fertilization, Nature, 457, 577–580, doi:10.1038/nature07716, 2009.

Price, N. M. and Morel, F. M. M.: Biological cycling of iron in the ocean, in: "Metal Ions in Biological Systems", Vol. 35, Iron Transport and Storage in Micro-organisms, Plants and Animals, Marcel Dekker, New York, 1–36, 1998.

Prospero, J. M., Ginoux, P., Torres, O., Nicholson, S. E., and Gill, T. E.: Environmental characterization of global sources of atmospheric soil dust identified with the Nimbus 7 Total Ozone Mapping Spectrometer (TOMS) absorbing aerosol product, Rev. Geophys., 40, 1002, doi:10.1029/2000RG000095, 2002.

Quéroué, F., Sarthou, G., Planquette, H. F., Bucciarelli, E., Chever, F., van der Merwe, P., Lannuzel, D., Townsend, A. T., Cheize, M., Blain, S., d'Ovidio, F., and Bowie, A. R.: High variability of dissolved iron concentrations in the vicinity of Kerguelen Island (Southern Ocean), Biogeosciences Discuss., submitted, 2014.

BGD
11, 17861–17923, 2014

Roquet, F., Park, Y.-H., Guinet, C., Bailleul, F., and Charrassin, J.-B.: Observations of the Fawn Trough Current over the Kerguelen Plateau from instrumented elephant seals, J. Marine Syst., 78, 377–393, doi:10.1016/j.jmarsys.2008.11.017, 2009.

Rosso, I. et al.: Vertical transport in the ocean due to sub-mesoscale structures: impacts in the Kerguelen region, Ocean Model., 80, 10–23, doi:10.1016/j.ocemod.2014.05.001, 2014.

Sanial, V., van Beek, P., Lansard, B., Souhaut, M., Kestenare, E., d'Ovidio, F., Zhou, M., and Blain, S.: Use of Ra isotopes to deduce rapid transfer of sediment-derived inputs off Kerguelen, Biogeosciences Discuss., 11, 14023–14061, doi:10.5194/bgd-11-14023-2014, 2014.

Sarmiento, J. L. and Gruber, N.: Carbon cycle. Chapter 8, in: "Ocean Biogeochemical Dynamics", Princeton University Press, Princeton, USA, ISBN: 9780691017075, 318–358, 2006.

Sarthou, G., Baker, A. R., Blain, S., Achterberg, E. P., Boye, M., Bowie, A. R., Croot, P., Laan, P., de Baar, H. J. W., Jickells, T. D., and Worsfold, P. J.: Atmospheric iron deposition and sea-surface dissolved iron concentrations in the eastern Atlantic Ocean, Deep-Sea Res. Pt. I, 50, 1339–1352, doi:10.1016/S0967-0637(03)00126-2, 2003.

Sarthou, G., Vincent, D., Christaki, U., Obernosterer, I., Timmermans, K. R., and Brussaard, C. P. D.: The fate of biogenic iron during a phytoplankton bloom induced by natural fertilisation: impact of copepod grazing, Deep-Sea Res. Pt. II, 55, 734, doi:10.1016/j.dsr2.2007.12.033, 2008.

Savoye, N., Trull, T. W., Jacquet, S. H. M., Navez, J., and Dehairs, F.: ^{234}Th-based export fluxes during a natural iron fertilization experiment in the Southern Ocean (KEOPS), Deep-Sea Res. Pt. II, 55, 841, doi:10.1016/j.dsr2.2007.12.036, 2008.

Schlitzer, R.: Carbon export fluxes in the Southern Ocean: results from inverse modelling and comparison with satellite-based estimates, Deep-Sea Res. Pt. II, 49, 1623–1644, doi:10.1016/S0967-0645(02)00004-8, 2002.

Schneider, B., Schlitzer, R., Fischer, G., and Nothig, E.-M.: Depth dependent elemental compositions of particulate organic matter (POM) in the ocean, Global Biogeochem. Cy., 17, 1032, doi:10.1029/2002GB001871, 2003.

Schroth, A. W., Crusius, J., Sholkovitz, E. R., and Bostick, B. C.: Iron solubility driven by speciation in dust sources to the ocean, Nat. Geosci., 2, 337–340, doi:10.1038/ngeo501, 2009.

SCOR Working Group: GEOTRACES – an international study of the global marine biogeochemical cycles of trace elements and their isotopes, Chem. Erde-Geochem., 67, 85–131, doi:10.1016/j.chemer.2007.02.001, 2007.

BGD
11, 17861–17923, 2014

Sedwick, P. N., Sholkovitz, E. R., and Church, T. M.: Impact of anthropogenic combustion emissions on the fractional solubility of aerosol iron: evidence from the Sargasso Sea, Geochem. Geophy. Geosy., 8, Q10Q06, doi:10.1029/2007GC001586, 2007.
Shaked, Y. and Lis, H.: Disassembling iron availability to phytoplankton, Front. Microbiol., 3, 123, doi:10.3389/fmicb.2012.00123, 2012.
Sherrell, R. M. and Boyle, E. A.: The trace metal composition of suspended particles in the oceanic water column near Bermuda, Earth Planet. Sci. Lett., 111, 155–174, doi:10.1016/0012-821X(92)90176-V, 1992.
Sokolov, S. and Rintoul, S. R.: Circumpolar structure and distribution of the Antarctic Circumpolar Current fronts: 1. Mean circumpolar paths, J. Geophys. Res., 114, C11018, doi:10.1029/2008JC005108, 2009.
Strzepek, R. F., Maldonado, M. T., Higgins, J. L., Hall, J., Safi, K., Wilhelm, S. W., and Boyd, P. W.: Spinning the "Ferrous Wheel": the importance of the microbial community in an iron budget during the FeCycle experiment, Global Biogeochem. Cy., 19, GB4S26, doi:10.1029/2005GB002490, 2005
Sunda, W. G. and Huntsman, S. A.: Iron uptake and growth limitation in oceanic and coastal phytoplankton, Mar. Chem., 50, 189–206, doi:10.1016/0304-4203(95)00035-P, 1995.
Tagliabue, A., Bopp, L., and Aumont, O.: Evaluating the importance of atmospheric and sedimentary iron sources to Southern Ocean biogeochemistry, Geophys. Res. Lett., 36, L13601, doi:10.1029/2009GL038914, 2009.
Tagliabue, A., Sallée, J.-B., Bowie, A. R., Lévy, M., Swart, S., and Boyd, P. W.: Surface-water iron supplies in the Southern Ocean sustained by deep winter mixing, Nat. Geosci., 7, 314–320, doi:10.1038/ngeo2101, 2014.
Tang, D. G. and Morel, F. M. M.: Distinguishing between cellular and Fe-oxide-associated trace elements in phytoplankton, Mar. Chem., 98, 18–30, doi:10.1016/j.marchem.2005.06.003, 2006.
Taylor, S. R. and McLennan, S. M.: The geochemical evolution of the continental crust, Rev. Geophys., 33, 241–265, doi:10.1029/95RG00262, 1995.
Tortell, P. D., Maldonado, M. T., and Price, N. M.: The role of heterotrophic bacteria in iron-limited ocean ecosystems, Nature, 383, 330–332, doi:10.1038/383330a0, 1996.
Trull, T. W., Davies, D., and Casciotti, K.: Insights into nutrient assimilation and export in naturally iron-fertilized waters of the Southern Ocean from nitrogen, carbon and oxygen isotopes, Deep-Sea Res. Pt. II, 55, 820–840, doi:10.1016/j.dsr2.2007.12.035, 2008.

BGD
11, 17861–17923, 2014

Trull, T. W., Davies, D. M., Dehairs, F., Cavagna, A.-J., Lasbleiz, M., Laurenceau, E. C., d'Ovidio, F., Planchon, F., Leblanc, K., Quéguiner, B., and Blain, S.: Chemometric perspectives on plankton community responses to natural iron fertilization over and downstream of the Kerguelen Plateau in the Southern Ocean, Biogeosciences Discuss., 11, 13841–13903, doi:10.5194/bgd-11-13841-2014, 2014.

Twining, B. S., Baines, S. B., Fisher, N. S., and Landry, M. R.: Cellular iron contents of plankton during the Southern Ocean Iron Experiment (SOFeX), Deep-Sea Res. Pt. I, 51, 1827–1850, doi:10.1016/j.dsr.2004.08.007, 2004.

van Beek, P., Bourquin, M., Reyss, J. L., Souhaut, M., Charette, M. A., and Jeandel, C.: Radium isotopes to investigate the water mass pathways on the Kerguelen Plateau (Southern Ocean), Deep-Sea Res. Pt. II, 55, 622–637, doi:10.1016/j.dsr2.2007.12.025, 2008.

van der Merwe, P., Bowie, A. R., Quéroué, F., Armand, L., Blain, S., Chever, F., Davies, D., Dehairs, F., Planchon, F., Sarthou, G., Townsend, A. T., and Trull, T.: Sourcing the iron in the naturally-fertilised bloom around the Kerguelen Plateau: particulate trace metal dynamics, Biogeosciences Discuss., 11, 13389–13432, doi:10.5194/bgd-11-13389-2014, 2014.

Wadley, M. R., Jickells, T. D., and Heywood, K. J.: The role of iron sources and transport for Southern Ocean productivity, Deep-Sea Res. Pt. I, 87, 82–94, doi:10.1016/j.dsr.2014.02.003, 2014.

Wagener, T., Guieu, C., Losno, R., Bonnet, S., and Mahowald, N.: Revisiting atmospheric dust export to the Southern Hemisphere ocean: biogeochemical implication, Global Biogeochem. Cy., 22, GB2006, doi:10.1029/2007GB002984, 2008.

Wedepohl, K. H.: The composition of the continental crust, Geochim. Cosmochim. Ac., 59, 1217–1232, doi:10.1016/0016-7037(95)00038-2, 1995.

Westberry, T. K., Behrenfeld, M. J., Milligan, A. J., and Doney, S. C.: Retrospective satellite ocean color analysis of purposeful and natural ocean iron fertilization, Deep-Sea Res. Pt. I, 73, 1–16, doi:10.1016/j.dsr.2012.11.010, 2013.

Zhang, Y., Lacan, F., and Jeandel, C.: Dissolved rare earth elements tracing lithogenic inputs over the Kerguelen Plateau (Southern Ocean), Deep-Sea Res. Pt. II, 55, 638–652, doi:10.1016/j.dsr2.2007.12.029, 2008.

Zhou, M., Zhu, Y., Dorland, R. D., and Measures, C. I.: Dynamics of the current system in the southern Drake Passage, Deep-Sea Res. Pt. I, 57, 1039–1048, doi:10.1016/j.dsr.2010.05.012, 2010.

BGD
11, 17861–17923, 2014

Zhou, M., Zhu, Y., d'Ovidio, F., Park, Y.-H., Durand, I., Kestenare, E., Sanial, V., Van-Beek, P., Queguiner, B., Carlotti, F., and Blain, S.: Surface currents and upwelling in Kerguelen Plateau regions, Biogeosciences Discuss., 11, 6845–6876, doi:10.5194/bgd-11-6845-2014, 2014.

BGD
11, 17861–17923, 2014

Table 1. Summary of iron standing stocks and fluxes for the upper mixed layer at KEOPS-2 process station sites R-2 (reference), A3 (plateau) and E (plume). For full details of the calculations, see text. Error bounds are provided where available. Due to logistical constraints resulting in missing data at some stations, we will focus on R-2, A3-2 and E-5 in the discussion. Data for stations A3-1, E-1 and E-3 are given to provide a context for spatial and temporal changes in the pools and fluxes during KEOPS-2.

Region	Reference	Plateau		Plume		
Station	R-2	A3-1	A3-2	E-1	E-3	E-5
Location	50°21.53′ S 66°42.44′ E	50°37.88′ S 72°4.99′ E	50°37.47′ S 72°03.35′ E	48°27.44′ S 72°11.26′ E	48°42.13′ S 71°58.1′ E	48°24.69′ S 71°53.99′ E
Mixed layer depth (m)[1]	76	165	123	64	32	39
Bottom depth (m)	2528	533	530	2057	1905	1920
Iron pools, integrated over the mixed layer (μmol m^{-2}, unless otherwise stated)						
dFe	7 ± 1	54 ± 10	21 ± 4	n.d.[2]	12 ± 0	2 ± 0
pFe	43 ± 0	1392 ± 195	401 ± 52	117 ± 1	n.d.[3]	61 ± 1
Biogenic pFe	9	13	14	11	n.d.	9
Lithogenic pFe	12	892	265	33	n.d.	9
POC (mmol m^{-2})	124 ± 11	239 ± 33	274 ± 24	198 ± 10	n.d.	150 ± 12
Iron fluxes (nmol m^{-2} d^{-1}, unless otherwise stated)						
(a) Diffusion	2	42	93	n.d.	1	0.5
(b) Upwelling	35	200	250	n.d.	330	140
(c) Entrainment	57	769	769	n.d.	330	330
(d) Total vertical dFe supply [a + b + c]	94	1011	1112	n.d.	661	471
(e) Lateral advective dFe supply	0		180		2400 ± 600	
Ratio of lateral-to-vertical supply [e/d]	0		0.2		4–5	
Atmospheric total Fe deposition			500 ± 390			
(f) Atmospheric soluble Fe deposition			50 ± 39			
Downward total pFe export flux	1302 ± 586[4]	n.d.	5746 ± 1198	4579 ± 1376	1890 ± 286	895 ± 358
(g) Downward non-lithogenic pFe export flux	–	–	2797 ± 583	–	–	541 ± 216
Downward POC export (mmol m^{-2} d^{-1})	1.8 ± 0.9[5]	n.d.	2.2 ± 0.7	7.0 ± 2.3	4.9 ± 1.5	2.0 ± 1.0
(h) Iron uptake[6]	40 ± 6	2528 ± 704	1120 ± 389	n.d.	743 ± 194	1745 ± 350
(i) Iron remineralization[7]	10 ± 2	19 ± 6	71 ± 12	27 ± 2	23 ± 2	31 ± 2

BGD
11, 17861–17923, 2014

Table 1. Continued.

Region	Reference	Plateau		Plume		
Station	R-2	A3-1	A3-2	E-1	E-3	E-5
	Fe/C ratios (mmol mol^{-1})					
(j) Mixed layer Fe/C cellular uptake ratio[8]	n.d.	n.d.	0.007 ± 0.004	n.d.	n.d.	0.021 ± 0.002
Suspended mixed layer particulate Fe_{tot}/C ratio[8]	0.2 ± 0.1	3.3 ± 0.4	1.5 ± 0.2	0.5 ± 0.1	n.d.	0.4 ± 0.1
Sinking Fe_{tot}/C export ratio	n.d.	n.d.	2.6 ± 1.0	0.7 ± 0.5	0.4 ± 0.3	0.5 ± 0.1
	Iron supply vs. demand (for reference R-2, plateau A3-2 and plume E-5 stations only) (nmol m^{-2} d^{-1})					
Total iron supply from "new" sources [d + e + f][9]	144	–	1342	–	–	2921
(k) Additional iron requirement to balance the dissolved budget [d + e + f – h + i][10]	114	–	293	–	–	1207
(l) Biological uptake of "new" iron [d + e + f – g][11]	–1158	–	–1455	–	–	2380
fe ratio [l/h][12]	–	–	–	–	–	1.4
Fe ratio [g/h][12]	–	–	–	–	–	0.3
	Estimated vs. observed production (mmol C m^{-2} d^{-1})					
Potential new primary production [l/j][13]	–	–	–	–	–	132
Observed net primary production[14]	11 ± 0	n.d.	158 ± 15	44 ± 4	57 ± 8	79 ± 9

n.d. = no data

[1] The mixed layer depths were calculated on the density plane to allow for heave (internal tides driven by topography) and other localised events.

[2] Due to logistical reasons there was no TMR cast for dFe at station E-1.

[3] Due to ISP failure, there were no mixed layer samples for pFe at station E-3.

[4] The P-trap was lost at R-2. We therefore estimated the pFe export flux using the ^{234}Th flux in suspended particles at 200 m (449 ± 203 dpm m^{-2} d^{-1}; from Table 1 in Planchon et al., 2014) and a mean Fe/Th ratio collected in the upper 200 m above the trap (2.9 ± 1.3 nmol dpm^{-1}).

[5] Estimated using the ^{234}Th flux and Fe/C ratio in suspended particles at 200 m.

[6] For stations R-2, A3-1, E-1 and E-3, seawater for iron uptake experiments were conducted for small cells filtered through a 25 µm mesh. This size-fraction represented between 77 and 91 % of the total POC pool. At stations A3-2 and E-5, we also used unfiltered seawater for our uptake experiments. Similar results were obtained for both the 0.2–25 µm and unfiltered fractions at station A3-2.

[7] Includes bacterial and mesozooplankton contributions.

[8] Mean of all samples collected in the mixed layer.

[9] Assumes only the soluble iron atmospheric supply is available (see text).

[10] A negative value indicates an additional iron requirement.

[11] At stations R-2 and A3-2, the negative values most likely occurred due to differences in the timescales of observations and calculations of fluxes (parameters were decoupled in time). The iron budget was based on an "instantaneous picture" of different fluxes that were not strictly measured at the same time (i.e., export fluxes operated on a different timeframe to the iron supply (vertical, lateral and atmospheric) and were very large at R-2 and A3-2).

[12] fe = uptake of new/uptake of new + regenerated iron and Fe = biogenic iron export/uptake of new + regenerated iron (Boyd et al., 2005). Note the fe and Fe ratios have considerable plasticity due to uncertainties in the lithogenic vs. biogenic fraction of exported particulate iron, and the missing iron source at A3-2.

[13] Calculated using the biological uptake of "new" iron (k) and molar Fe/C cellular uptake ratio (j).

[14] Net primary production (NPP) integrated within the euphotic zone down to 1 % PAR, based on ^{13}C incorporation (Cavagna et al., 2014).

BGD
11, 17861–17923, 2014

Table 2. Fluxes of iron and carbon exported in sinking particles (trap deployed at 200 m) and ratio of Fe/C in sinking (traps) and suspended mixed layer (ISP) particles at stations A3-2 and E-stations. There was no successful trap deployment at station R-2. A comparison to previous experiments is provided.

Site	PFe flux ($\mu mol\, m^{-2}\, d^{-1}$)		POC flux ($mmol\, m^{-2}\, d^{-1}$)		Fe/C (sinking) ($mmol\, mol^{-1}$)		Fe/C (suspended) ($mmol\, mol^{-1}$)
	mean	SD	mean	SD	mean	SD	mean
KEOPS-2							
A3-2	5.75	1.20	2.23	0.68	2.57	0.97	1.51
E-1	4.58	1.38	7.02	2.28	0.65	0.52	0.49
E-3	1.89	0.29	4.87	1.54	0.39	0.29	0.39
E-5	0.90	0.36	2.00	1.00	0.45	0.13	0.33
KEOPS-1[1]							
A3-initial	0.33	0.05	3.60	0.43	0.09	–	–
A3-final	0.20	0.02	1.36	0.39	0.15	–	–
C5	1.51	0.32	1.57	0.08	0.96	–	–
CROZEX[2]							
North	0.84	–	15.9	–	2.55	–	0.69
South	0.23	–	12.9	–	0.57	–	0.31
SAZ-Sense[3]							
P1	0.17	0.09	3.34	1.81	0.05	0.04	0.04
P2	0.07	0.01	2.11	0.88	0.04	0.02	0.06
P3	0.21	0.05	0.86	0.38	0.25	0.13	0.03
FeCycle-1[4]							
F1-80 m	0.22	0.03	n.d.	–	n.d.	–	0.04
F1-120 m	0.36	0.05	2.09	0.03	0.17	–	–
F2-80 m	0.55	0.06	2.51	0.17	0.22	–	–
F2-120 m	0.35	0.03	2.10	0.01	0.17	–	–

BGD
11, 17861–17923, 2014

Table 2. Continued.

Site	PFe flux (μmol m^{-2} d^{-1}) mean	SD	POC flux (mmol m^{-2} d^{-1}) mean	SD	Fe/C (sinking) (mmol mol^{-1}) mean	SD	Fe/C (suspended) (mmol mol^{-1}) mean
FeCycle-2[5]							
A1-100 m	5.	0.7	11	–	0.45	–	0.78
A1-200 m	7.3	1.6	5.8	–	1.26	–	–
A2-100 m	10	1.0	42	–	0.24	–	1.12
A2-200 m	10	9	6.8	1.8	1.47	–	–
A3-100 m	17	2	12	2	1.42	–	0.63
A3-200 m	10	1	14	–	0.71	–	–
A4-100 m	20	8	9.3	0.9	2.15	–	0.86
A4-200 m	15	6	6.1	1.8	2.46	–	–
Other literature data							
Mixed plankton assemblages[6]	–	–	–	–	–	–	0.01–0.05
Iron limited algae[7]	–	–	–	–	–	–	0.01
Iron replete algae[7]	–	–	–	–	–	–	0.02–0.05
Southern Ocean synthesis[8]	–	–	–	–	0.01–0.06	–	–

n.d. = no data

[1] Data for particles > 0.2 µm (Blain et al., 2007; Bowie et al., unpublished data).

[2] Data for > 53 µm particles only (Planquette et al., 2011). Downward Fe fluxes were estimated from samples collected from in situ pumps using ^{234}Th depletions and Fe/Th ratios in sinking particles. Waters to the north of Crozet Island were "downstream" of the islands and iron fertilised, whilst those to the south were "upstream" HNLC conditions. The Fe/C from bioassay culturing experiments conducted during CROZEX was 0.25 mmol mol^{-1} (Moore et al., 2008).

[3] Data for particles > 1 µm (Bowie et al., 2009).

[4] Data for particles > 0.4 µm (Frew et al., 2006). Only 1 mixed layer Fe/C ratio was reported. The biogenic Fe/C mixed layer ratio was estimated to be 0.004–0.012 mmol mol^{-1}.

[5] Data for particles > 0.4 µm, except deployment A1 (> 2 µm) (Ellwood et al., 2014). The mixed layer Fe/C ratios were calculated from Table 4 using the sediment traps deployment periods reported in Table 3 in the original publication.

[6] Estimates of Fe/C for diatoms and whole plankton assemblages compiled by de Baar et al. (2008), with optimal ratios for growth tending towards the upper end of the range.

[7] Intracellular ratio reported for HNLC polar water south of New Zealand during SOFeX (Twining et al., 2004).

[8] Ratio of dFe supply to POC export, synthesis by Morris and Charette (2013).

BGD
11, 17861–17923, 2014

Table 3. Iron regeneration rates based on bacterivore and herbivore contributions.

Site	Bacterial ($pmol\,L^{-1}\,d^{-1}$)	Mesozooplankton ($pmol\,L^{-1}\,d^{-1}$)	Total Fe regeneration ($pmol\,L^{-1}\,d^{-1}$)	% bacterial contribution	Total integrated mixed layer Fe regeneration ($nmol\,m^{-2}\,d^{-1}$)
R-2	0.06 ± 0.01	0.04	0.10	61	10
A3-1	0.10 ± 0.03	0.02	0.12	87	19
A3-2	0.43 ± 0.07	0.03	0.46	93	71
E-1	0.33 ± 0.02	0.04	0.37	88	27
E-3	0.54 ± 0.04	0.06	0.60	90	23
E-5	0.59 ± 0.03	0.08	0.67	88	31

BGD
11, 17861–17923, 2014

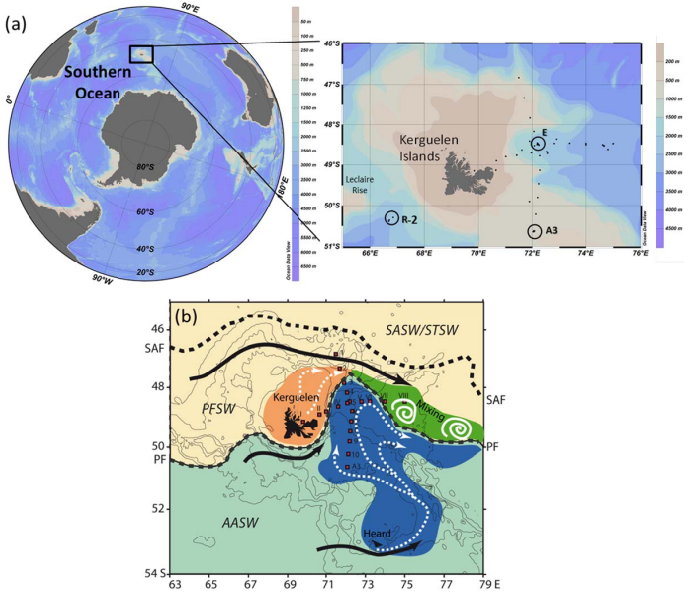

Figure 1. (a) The location of the KEOPS-2 study in the Indian sector of the Southern Ocean showing bathymetry around the Kerguelen archipelago. Our biogeochemical iron budgets focus on three process stations (open black circles): reference R-2 (50°2′ S, 66°4′ E), plateau A3 (50°4′ S, 72°0′ E) and plume E (48°3′ S, 72°1′ E). Black dots mark the positions of the other stations visited, including N–S and E–W survey transects at the start of the KEOPS-2 expedition (Blain et al., 2014a). **(b)** A schematic of the mean regional circulation of surface/subsurface waters around the Kerguelen archipelago, indicating circumpolar Southern Ocean fronts, locations of stations conducted along N–S and E–W transects, and pathways and origins of different water masses flowing on the plateau and offshore into the plume. The abbreviations are Antarctic Surface Water (AASW), Polar Frontal Surface Water (PFSW), Subantarctic Surface Water (SASW), and Subtropical Surface Water (STSW), subantarctic front (SAF), polar front (PF) (reproduced with permission from Park et al., 2014a, courtesy of Isabelle Durand and Young-Hyang Park, LOCEAN/DMPA, MNHN, Paris).

BGD
11, 17861–17923, 2014

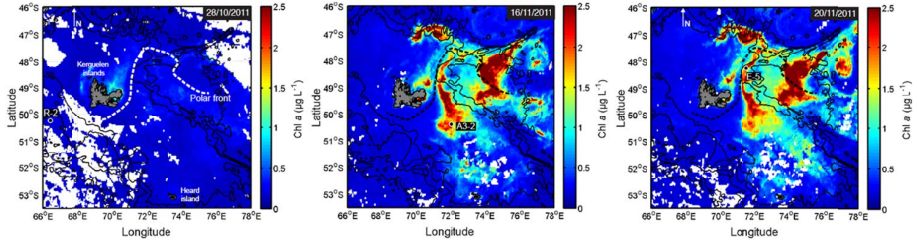

Figure 2. MODIS ocean-colour satellite images showing the development of the plateau and plume blooms during the KEOPS-2 study. Surface chlorophyll ($\mu g\,L^{-1}$) biomass is shown for the nearest clear sky day to the final sampling day at stations R-2 **(a)**, A3-2 **(b)** and E-5 **(c)**. The polar front is shown as a black dashed line. Trull et al. (2014) discuss the timing of the stations relative to bloom development.

BGD
11, 17861–17923, 2014

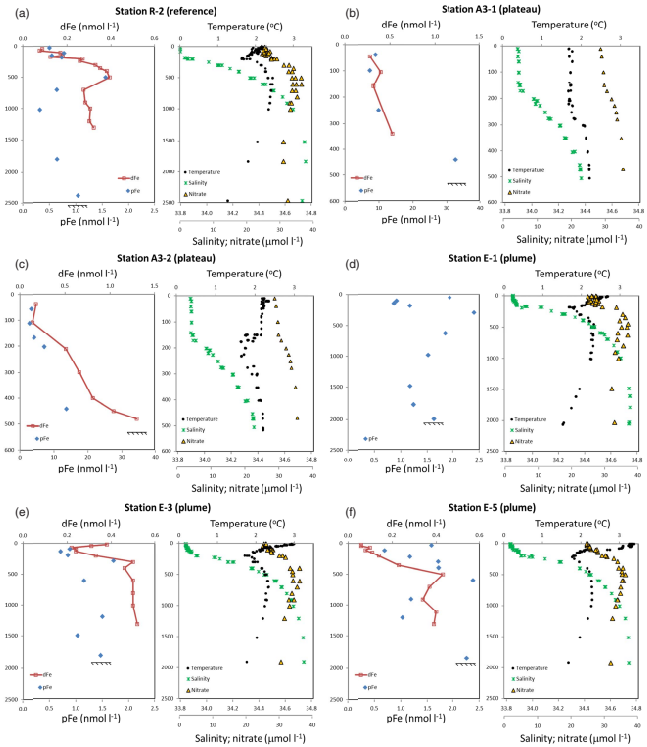

Figure 3. (a) Vertical profiles of dissolved iron (dFe) and particulate iron (pFe), temperature, salinity and nitrate at reference station R-2. The seafloor depth at 2528 m is shown. **(b, c)** Vertical profiles of dFe and pFe, temperature, salinity and nitrate at plateau stations A3-1 and A3-2. The seafloor depth at ~ 530 m is shown. Note different scales for dFe and pFe compared to R-2 and E stations. **(d–f)** Vertical profiles of dFe and pFe, temperature, salinity and nitrate at plume stations E-1 , E-3 and E-5. The seafloor depth ranging from 1905 m (E-3) to 2057 m (E-1) is shown.

BGD
11, 17861–17923, 2014

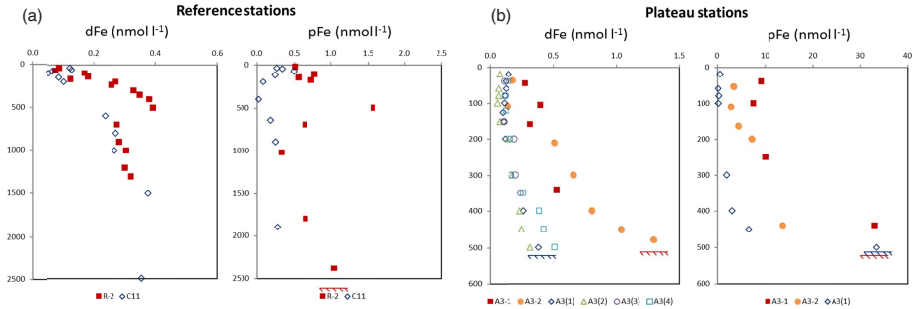

Figure 4. (a) Comparison of dFe and pFe at reference stations for KEOPS-1 (station C11, open blue diamonds) and KEOPS-2 (station R-2, closed red squares) studies. The water depths were 3110 m at C11 and 2530 m at R-2. **(b)** Comparison of dFe and pFe at A3 plateau stations for KEOPS-1 (open symbols) and KEOPS-2 (closed symbols) studies. Data are shown for all visits to A3 on both KEOPS cruises. Note difference scale for dFe and pFe between **(a)** and **(b)**.

BGD
11, 17861–17923, 2014

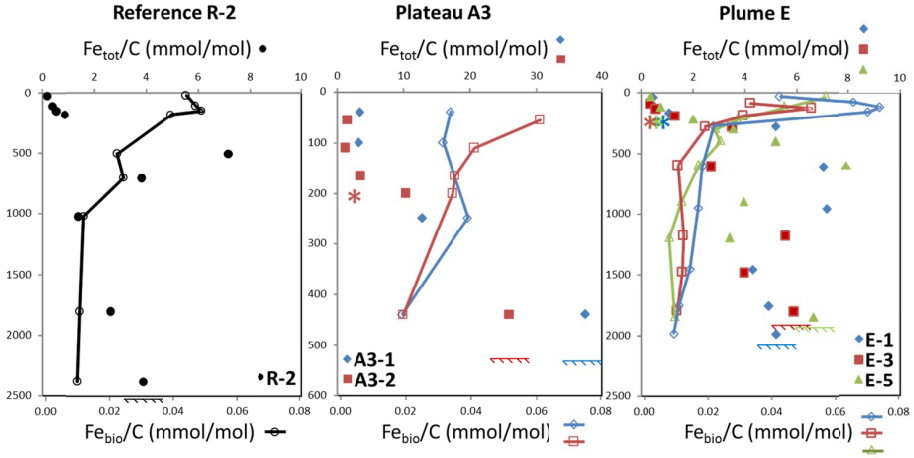

Figure 5. Vertical profiles of Fe/C ratios in suspended (ISP) and sinking (P-trap) particles. Solid symbols indicate Fe_{tot}/C (i.e., ratio of biogenic + lithogenic Fe over POC) and joined open symbols indicate Fe_{bio}/C (i.e., ratio of biogenic Fe only over POC; calculated using P as a normaliser). The asterisk markers (∗) show the export Fe_{tot}/C ratio (P-traps). Note the different scale on the *x* axis for Fe_{tot}/C at A3 stations.

BGD
11, 17861–17923, 2014

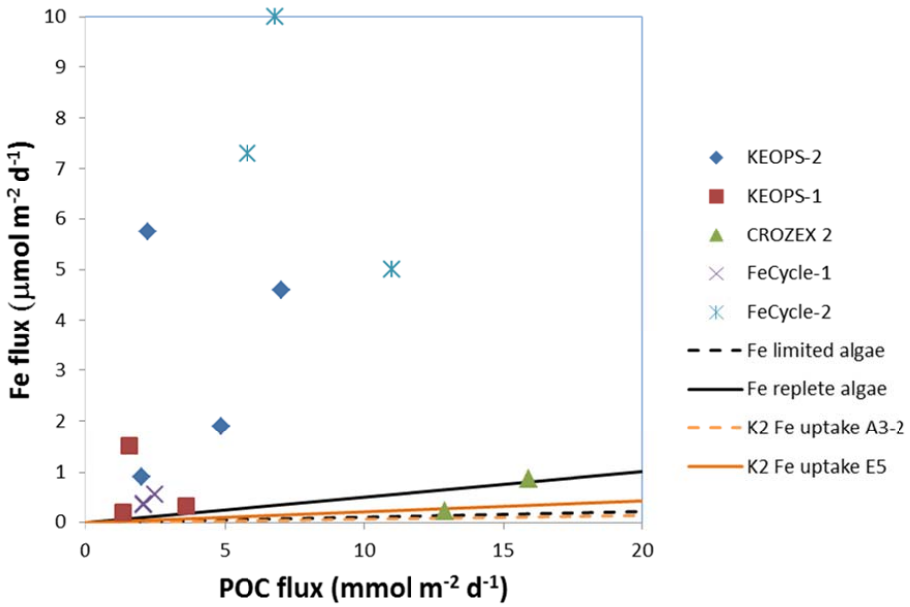

Figure 6. A comparison of export fluxes of pFe vs. POC in sinking particles for natural iron fertilisation studies in the Southern Ocean. For details of the sampling methods, refer to Table 2 and the original articles. The lines indicate Fe/C ratios for Fe limited (black dashed) and Fe replete (black solid) phytoplankton (Twining et al., 2004), and the mean mixed layer intracellular Fe/C ratios at stations A3-2 (orange dashed) and E-5 (orange solid) on KEOPS-2 (taken from Table 1). FeCycle-2 had complex biogeochemical dynamics due to a storm event and subsequent deep water mixing (during sediment trap deployment A3), splitting the study into two phases ("eddy centre" and "eddy periphery"). To aid interpretation of Fe/C export data in the context of iron fertilisation, only data from the pseudo Lagrangian phase 1 (i.e., deployments A1 and A2 during bloom development and export) from that study is included in this plot (Ellwood et al., 2014).

BGD
11, 17861–17923, 2014

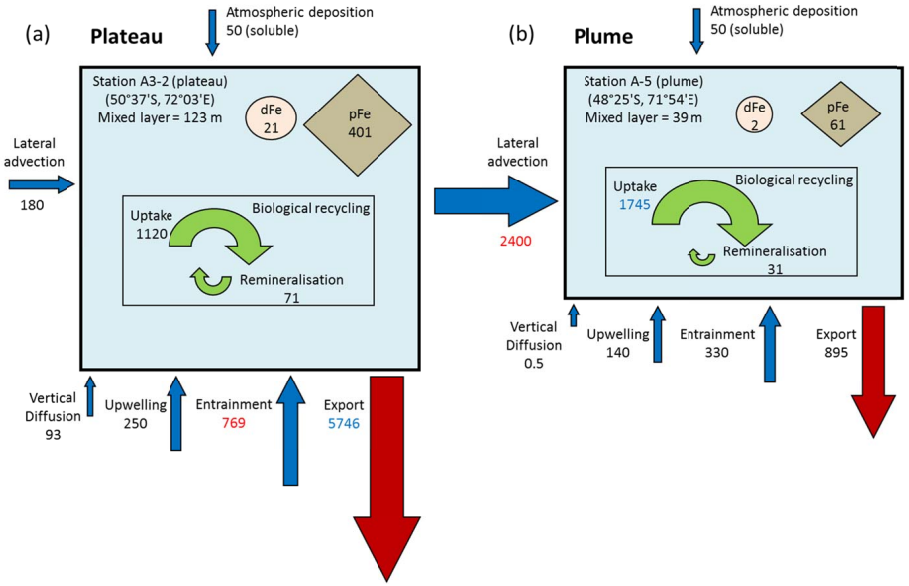

Figure 7. Biogeochemical iron budgets for the plateau (A3-2, **a**) and plume (E-5, **b**) stations. Iron pools are given in $\mu mol\,m^{-2}$ and iron fluxes in $nmol\,m^{-2}\,d^{-1}$. The major Fe sources are shown in red text and the major Fe sinks in blue text. The size of the arrows is roughly proportional to the magnitude of the Fe fluxes.

BGD
11, 17861–17923, 2014